Oxygen Release Degradation in Li-ion Battery Cathode Materials: Mechanisms and Mitigating Approaches

Soroosh Sharifi-Asl [a], Jun Lu [b, *], Khalil Amine [b, *], Reza Shahbazian-Yassar [a, *]

[a] Mechanical and Industrial Engineering Department, University of Illinois at Chicago, Chicago, Illinois 60607, United States.
[b] Chemical Science and Engineering Division, Argonne National Laboratory, 9700 S. Cass Avenue, Argonne, Illinois 60439, USA

* Correspondence to: junlu@anl.gov, amine@anl.gov, rsyassar@uic.edu

Keywords: Li-ion Battery Cathodes, Oxygen Release, Thermal Runaway, Structural Degradation, Phase Transformation.

Abstract:

Widespread application of Li-ion batteries (LIBs) in large scale transportation and grid storage systems requires highly stable and safe performance of the batteries in prolonged and diverse service conditions. Oxygen release from oxygen-containing positive electrode materials is one of the major structural degradations resulting in rapid capacity/voltage fading of the battery and triggering the parasitic thermal runaway events. Herein, we summarized the recent progress in understanding the mechanisms of the oxygen release phenomena and corelative structural degradations observed in four major groups of cathode materials: layered, spinel, olivine and Li-rich cathodes. In general, the hybridization of undercoordinated oxygen atoms that leads to O_2 formation and evolution accompanied by phase transitions is regarded as the triggering mechanism for cathodes oxygen release. Layered oxide $LiMO_2$ cathodes are known to be more prone to oxygen release, and composition design, particularly Ni content plays a significant role in their structural stability. Cationic substitution of transition metals with extra Li-ions activates the anionic redox reaction that adversely affects the structural stability and causes rapid oxygen release during cycling. Spinel $LiMn_2O_4$ cathodes have a higher oxygen stability compared to the layered oxide cathodes but suffer from Mn dissolution and fast capacity fading. While partial substitution of Mn with Ni alleviates the Mn dissolution, it deteriorates the oxygen stability of the spinel cathodes. Olivine phase $LiFePO_4$ cathodes are highly stable and do not release substantial O_2 at elevated temperatures, however isostructural $LiMnPO_4$ and $LiCoPO_4$ olivine cathodes suffer from structural instability and rapid oxygen release. In addition, the engineering and materials design approaches that improve the structural integrity of the cathode materials and minimize the detrimental O_2 evolution reaction have been summarized. We believe that this review can guide researchers on developing mitigation strategies for the design of next generation oxygen-containing cathode materials where the oxygen release is no longer a major degradation issue.

1. Introduction:

High energy density Li-ion batteries (LIBs) hold the key for enabling the next generation of sustainable and green energy technologies[1–5]. Oxygen-containing cathodes are the main constituents enabling high voltage, high energy density Li-ion batteries. Since graphite is utilized as the negative electrode in most of the commercialized LIBs, electrochemical properties such as energy density and operating voltage of the cells are defined by the choice of cathode materials. For instance, the charge voltage, which is limited by the top of the anion-p bands of the cathode, can be expanded by replacing an oxide ion with polyanions[6]. However, such changes impact the Li-ion intercalation mechanism, electron conductivity and importantly structural stability of the cathode material[7]. Generally, the LIB cathode materials are transition metal oxides or phosphates that are designated as the reservoir of the Li ions in the batteries. Cubic closed packed array of oxygen framework allows for unrestricted shuttling of Li-ions in the layered and spinel phase oxide structures[8]. Also, oxygen atoms coordinate the phosphorous atoms to form $(PO_4)^{-3}$ polyanions, which are the building blocks of the olivine cathodes structure[9]. Structural instability of such oxygen-containing cathodes can lead to release of the cathode lattice oxygen in form of O_2[10]. Extensive oxygen release leads to severe degradation of the cathode performance and jeopardizes the safety of the battery by triggering a thermal runaway event, in which the battery catches fire and rapidly releases a large amount of uncontrolled heat and energy[11]. Thermal runaway events have been observed in several Li-ion battery powered systems ranging from laptop and cell phones to e-cigarettes, headphones, electric vehicles and even airplanes, and have caused serious injuries to the consumers[12,13]. It was found that the thermal runaway is the outcome of a series of self-progressive exothermic events triggered by an external stimulus such as ambient temperature rise or mechanical impact, or caused by an internal stimulus such as short circuit, overcharge or applied high current rates[14,15]. The occurrence and sequence of these chain of events can vary based on the materials design and the specific conditions that trigger the thermal runaway reaction[16]. The schematic Figure 1A, schematically illustrates the general mechanisms identified for thermally triggered / overcharge-induced thermal runaway reaction. Prevalently, external causes such as local temperature rise can initialize the undesired reactions that lead to the thermal runaway. If the battery temperature is increased to above 90 °C, the exothermic breakdown of the solid electrolyte interphase (SEI) formed on the graphite anode can further increase the temperature to above 120 °C[17,18]. Meanwhile, the SEI breakdown triggers the side reactions between the unprotected anode and the alkyl carbonate electrolyte, leading to formation of combustible gases such as ethane and methane[17]. At this point the polymer separator will melt down, causing a short circuit between the positive and negative electrodes that rapidly increases the temperature and expands the area of heat dissipation in the battery[6]. Finally, at above 150 °C the oxide cathode material decomposes and releases a large amount of oxygen that can ignite the flammable electrolyte/combustible gases in presence of the accumulated heat and triggers the thermal runaway of the battery[16]. Noteworthy, it has been identified that the thermal runaway reaction can occur without an internal short circuit caused by the separator meltdown. In this case, it is observed that if the temperature of an NMC/graphite battery exceeds 115.2 °C by ambient temperature rise, even without the separator break-down and the resultant short circuit, a chemical crosstalk between the cathode and the anode can release a large amount of heat that increases the temperature to □800 °C and eventually leads to the ignition of the battery[19]. These observations further stress the significant role of the oxygen release from the cathode materials in the safety aspects of LIBs[20]. Overcharge-induced failure can be regarded as another scenario for thermal runaway reactions [21,22]. In this scenario, the lithiation of the graphite anode beyond its intercalating capacity leads to deposition

of metallic Li on the graphite particles surface[23]. This results in SEI thickening and increased cell resistance, which will lead to Joule heating of the battery components[24]. In addition, the anode/the cathode will become reducing/oxidizing agents by continuous insertion/extraction of electrons and can trigger exothermic side reactions with the unstable electrolyte[25]. Subsequently decomposition of electrolyte will result in combustible gas formation that leads to battery swelling and further increase in the battery resistance[26]. As the temperature increases gradually, the anode SEI decomposition can lead to exothermic reaction of lithiated graphite with the electrolyte that further increases the temperature. Subsequently the overcharged cathode that is highly susceptible to thermal decomposition, will break down and release oxygen [21,22]. This is due to the fact that charging the cathodes beyond the energy of oxygen 2p band structure can generate peroxo-like oxygen species that can form O-O bonds and evolve as O_2 gas (Figure 1B)[27,28]. Similarly, local heating of the overcharged cathodes can trigger the migration of transition metal cations by breaking TM-O bonds. This leads to O-O bond formation between the undercoordinated oxygen atoms and results in the parasitic oxygen release that is explained in length throughout the article with regards to specific cathode systems (Figure 1C) [29–33].

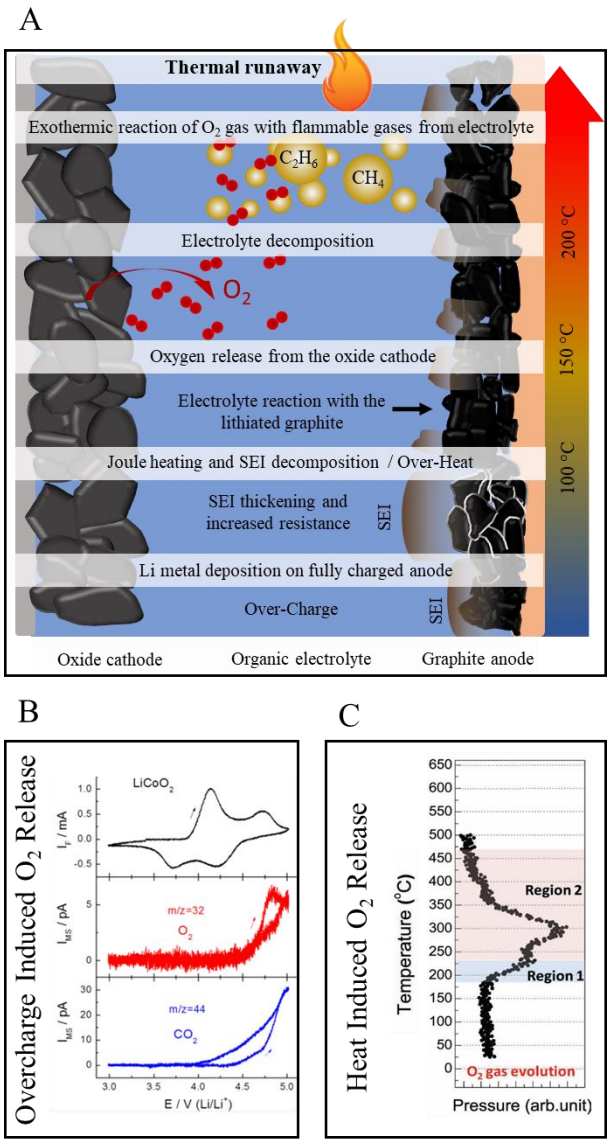

Figure 1. (A) Schematic illustration of the chain of events in a thermal runaway reaction. Over-charging the cell leads to Li deposition on graphite particles and SEI thickening. This will increase the cell resistance and leads to Joule heating. A local temperature rise to above 90 °C, either caused by Joule heating, or due to ambient temperature increase, would result in the exothermic breakdown of the SEI layer, which further increases the temperature to above 120 °C. Then the polymer separator melts down and causes a short circuit, which further increase the temperature. Finally, the cathode material decomposes and releases a large amount of oxygen that can ignite the combustible gases and flammable electrolyte and trigger the thermal runaway reaction. **(B)** Mass spectroscopy results demonstrating two possible routes for oxygen evolution from cathodes demonstrating O_2 release from $LiCoO_2$ when charged over 4.4 V, which is beyond the energy level of the O-2p bands in layered oxide cathodes: Reproduced with permission.[28] Copyright 2014, American Chemical Society. **(C)** Oxygen release during thermal decomposition of charged NMC cathodes as a result of hybridization of undercoordinated oxygen atoms accompanied with spinel and rock-salt phase transformations: Reproduced with permission[33]Copyright 2012, Wiley-VCH.

Employing a range of characterization techniques at the bulk-scale such as in-situ calorimetry[34,35], in–operando high energy synchrotron X-ray tomography and radiography[36,37], it was discovered that the onset temperature and the extent of the thermal runaway reaction is highly dependent on the type and composition of the positive electrode materials[34]. Therefore, the cathodes oxygen release phenomenon have been closely investigated by various means such as thermal analysis[38], time resolved x-ray diffraction (TR-XRD)[39], Raman spectroscopy[40–43], in-situ differential electrochemical mass spectroscopy (DEMS)[28,44,45], x-ray absorption spectroscopy (XAS)[33,46–50], in-situ transmission electron microscopy (TEM)[51–55] and computational modeling [56,57]. The methods that have been employed for studying the LIBs thermal runaway and cathodes degradation reaction are schematically depicted in the Figure 2.

Despite the numerous challenges associated with studying the cathode materials such as the structural complexity of the cathode materials[58,59], particle to particle variation caused by gradient state of charge in the electrodes[52,60], the interplay of several degradation mechanisms[61,62] and the sensitivity to various experimental conditions such as the atmosphere[63,64] and electron probe[65–67], great progress in understanding and improving their structural stability have been achieved in the past few years. However, the oxygen release from cathode materials still remains as one of the key degradation issues of oxygen-containing cathodes. Thus, herein we have reviewed and summarized the oxygen release degradation mechanisms of the widely used cathode materials such as (1) layered $LiMO_2$ (M = Fe, Mn, Co) cathodes; (2) spinel LiM_2O_4 (M=Ni, Mn) cathodes; (3) olivine $LiMPO_4$ (M = Fe, Mn, Co) cathodes; and (4) Li-rich NMC cathodes. It is concluded that the O_2 evolution is a complex mechanism that is influenced by many parameters such as state of charge (SOC), morphology and size of the particles, chemical composition and atomic arrangements of the cathodes. Additionally, proposed solutions and approaches utilized to improve the cathodes degradation and alleviate the oxygen release reaction are categorized and reviewed in the following sections.

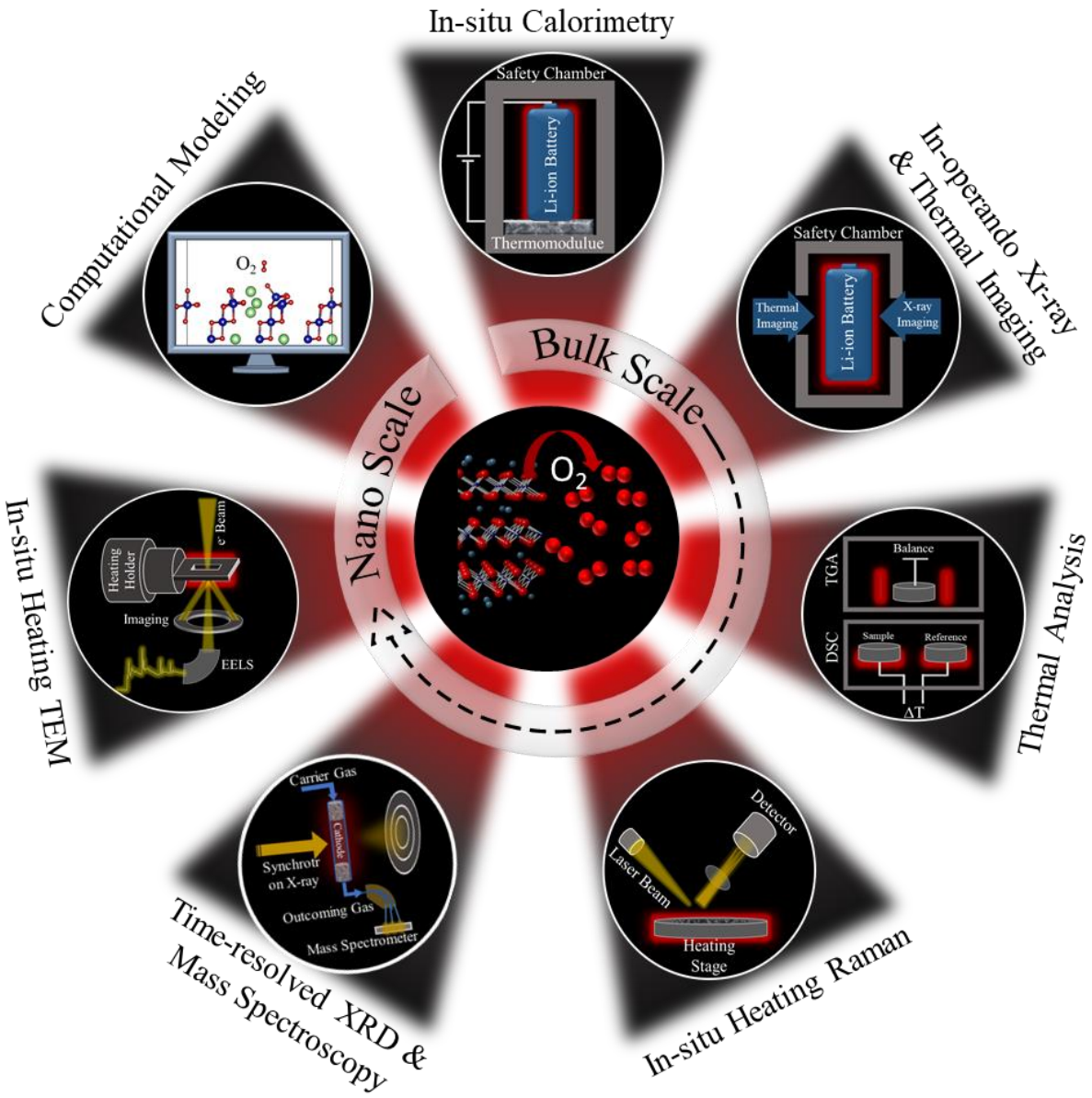

Figure 2. Schematic illustration of the methods used to study the oxygen-release induced degradation of cathode materials ranging from bulk to nanoscale.

2. Mechanisms of Cathodes Degradations:

2.1. Layered Oxide Cathodes:

2.1.1. $LiMO_2$ (M = Co & Ni). Layered oxide cathode materials that enabled the commercialization of Li-ion batteries are composed of cubic close packed (CCP) oxygen arrays with metal ions occupying octahedral sites, which form consecutive LiO_2 and MO_2 layers[68,69]. Isostructural $LiCoO_2$ and $LiNiO_2$ share the crystal structure of α-$NaFeO_2$ with $R\bar{3}m$ space group where the Li/M ratio is 1 or less in these structures. $LiCoO_2$ was proposed by Goodenough before the discovery of Li-ion batteries in 1980's[70]. The reversible shuttling of Li-ions throughout the electrochemical cycling in between the MO_2 layers is the advantageous characteristic of the layered oxide cathodes. However, since there are several phases viable as a function of Li/M ratio, electrochemical

delithiation higher than a certain extent can result in irreversible phase transitions, which leads to rapid capacity fading of the $LiMO_2$-based batteries. The charge voltage of the layered oxide cathodes is manually limited by the energy of the top of O-2p bands. This is because charging beyond this limit (ca. 4.6 V) will result in peroxide $(O_2)^{2-}$ formation and release of O_2 and/or insertion of protons into the cathodes structure[27], which has been quantified experimentally[28] (Figure 3A). Additionally, high extent of delithiation (high cut-off voltage charging) can promote the glide of partial dislocations, and provides a path for transition metal migration to the Li octahedral sites that leads to formation of the spinel phase[71,72]. Spinel phase formation and oxygen release has been observed primarily at the surface of the cycled particles (Figure 3B)[29–32]. This is explained by the electrochemically induced Li deficiency at the surface and inhomogeneous Li distribution throughout the cathode particles[29,73]. In addition to cycling induced oxygen release, thermal treatment of the layered oxide cathode results in the structural decomposition of the $LiMO_2$ cathodes[74]. At pristine state, $LiCoO_2$ is known to be stable up to 900 °C, however partial delithiation results in the formation of under-coordinated oxygen atoms, that can form O-O bonds and release at around 200 °C[38]. The oxygen release reaction results in the formation of the electrochemically inactive phases with less oxygen in their stoichiometry[75]. The following reaction is suggested to explain the oxygen evolution mechanism from Li_xCoO_2.

$$Li_xCoO_2 \rightarrow \frac{1-x}{3}Co_3O_4 + xLiCoO_2 + \frac{1-x}{3}O_2 \quad (1)$$

Additionally, it is suggested that the activation energy of oxygen release is a function of the state of charge (SOC) and the extent of delithiation, so further delithiation reduces the activation energy and further destabilizes the structure[74]. Also, it is shown that increasing the surface area destabilizes the Li_xCoO_2 structure and increases the extent of oxygen release (Figure 3C)[75,76]. Recently, utilizing in-situ heating TEM, the effect of particle surface fraction on the thermal instability of $LiCoO_2$ was explained[77] (Figure 3D). The results based on scanning transmission electron microscopy and electron energy loss spectroscopy (STEM/EELS), together with ab-initio molecular dynamic simulation (AIMD) revealed that oxygen release reaction is dominant at the surface of Li_xCoO_2 particles, in specific facet terminations. Also, a two-step phase transition that results in the sequential formation of spinel and rock-salt phases at the surface of Li_xCoO_2 particles was identified. Therefore, based on the experimental observations the following decomposition reaction for Li_xCoO_2 was proposed.

$$Li_xCoO_2\ (\text{layered}) \longrightarrow Li_xCoO_2\ (\text{layered}) + Li_xCo_{3-x}O_4\ (\text{spinel}) + \varepsilon O_2 \longrightarrow Li_xCoO_2\ (\text{layered}) + Li_xCo_{3-x}O_4\ (\text{spinel}) + Li_xCo_{1-x}O\ (\text{rock-salt}) + \delta O_2 \quad (2)$$

where, ε and δ values depend on the surface facet termination and particle morphology. It has been identified that such phase transitions generate a stress field at the surface of cathode particles, which can affect the oxygen evolution kinetics. In particular, by including elastic energy density to the free energy functional describing the oxygen release, an alteration of oxygen release at the rock-salt/gas-phase interface can be observed[56].

Moreover, owing to thermodynamic instability of unpaired e_{2g} electrons in high valence Ni ions and Jahn-Teller distortion phenomenon, Li_xNiO_2 is even more structurally unstable compared to Li_xCoO_2[38]. Meaning that at the same SOC, a relatively lower temperature is required to trigger the oxygen release reaction in Li_xNiO_2[78]. Interestingly, thermal decomposition of Ni based cathodes has been shown to proceed to the extent that pure Ni nano-particles form on the surface of the cathodes at elevated temperatures[52]. These observations, carried out by in-situ heating TEM technique, further reveal the higher extent of oxygen release in the thermal decomposition reaction of Ni based layered oxide cathodes.

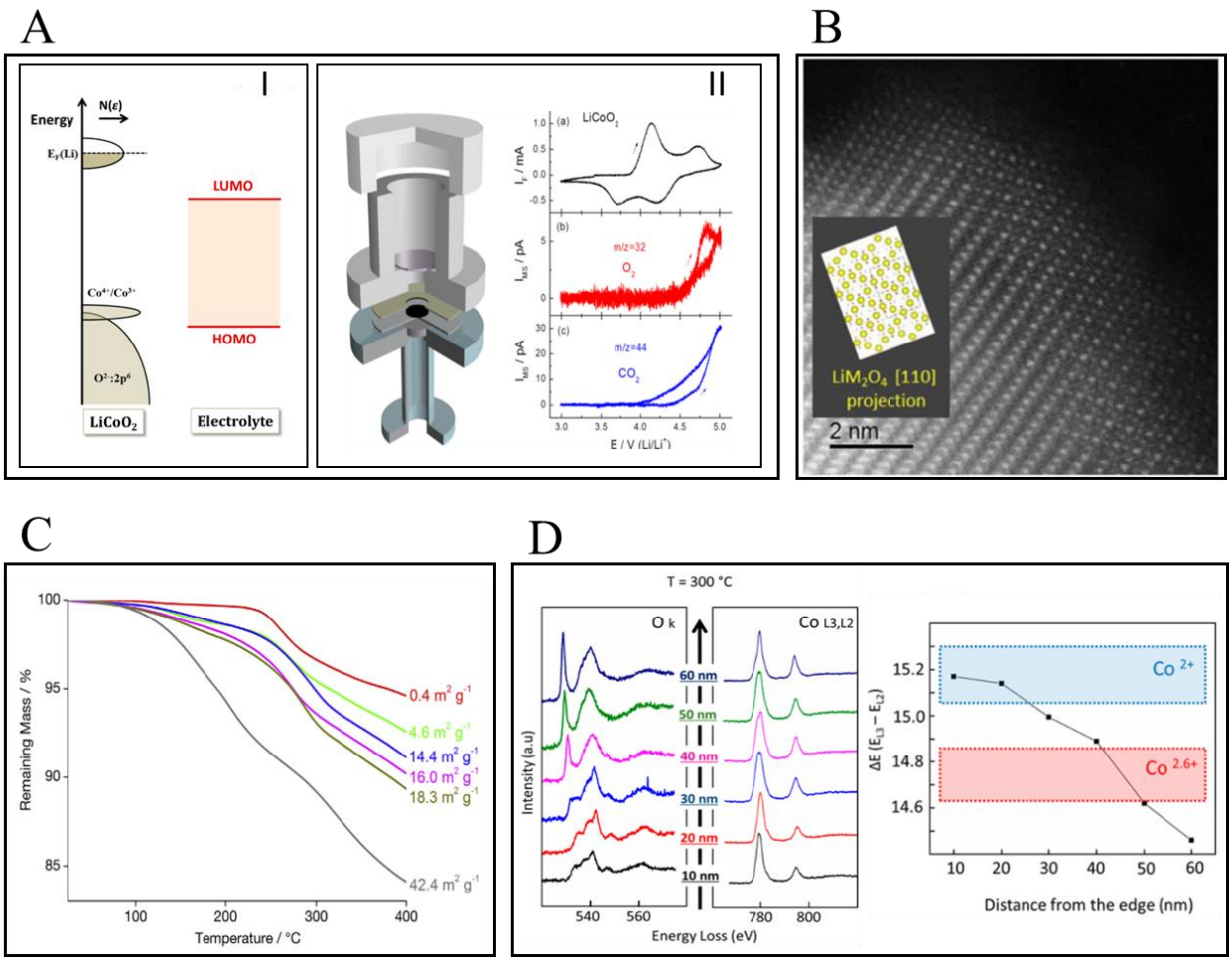

Figure 1. General depiction of the O_2 release mechanisms for $LiCoO_2$ cathodes (A) (I) Schematic energy diagram of $LiCoO_2$ and Li, with respect to the highest occupied molecular orbital (HOMO) and lowest unoccupied molecular orbitals (LUMO) of a carbonate-based electrolyte: Reproduced with permission.[27] Copyright 2013, American Chemical Society , (II) experimental illustration of oxygen release at overcharge condition captured by DEMS experiment: Reproduced with permission.[28] Copyright 2014, American Chemical Society. **(B)** Surface degradation and phase transition of $LiCoO_2$ upon cycling: Reproduced with permission.[29] Copyright 2017, Electrochemical Society. **(C)** Thermal analysis results demonstrating the effect of active material surface area on the thermal decomposition extent of Li_xCoO_2: Reproduced with permission.[75] Copyright 2014, Elsevier. **(D)** *In-situ* EELS results showing the role of the surface area on the thermal instability of Li_xCoO_2: Reproduced with permission.[77] Copyright 2017, American Chemical Society.

2.1.2. $LiNi_{1-x-y}Co_yAl_xO_2$ (NCA) and $LiNi_{1/3}Co_{1/3}Mn_{1/3}O_2$ (NMC). To improve the structural and thermal stability of high capacity layered oxide cathode materials, alloying approach has been regarded as a promising solution. To this end, $Li(Ni_xMn_yCo_z)O_2$ (NMC) and $Li(Ni_{0.8}Co_{0.15}Al_{0.05})O_2$ (NCA) cathodes were successfully synthesized and commercialized[79]. The NCA and NMC cathodes are considered as solid solutions of $LiNiO_2$, $LiCoO_2$ and $LiMnO_2$ that retain the layered $R\bar{3}m$ structure[80]. These materials have superior properties such as better Li-stoichiometry (decreased cation mixing in Li layer), improved electrochemical performance and higher thermal stability compared to $LiNiO_2$ and $LiCoO_2$[81–83]. Therefore, they are dominating the market of high capacity and large scale Li-ion batteries, such as electric vehicles[80,84,85]. The redox

active centers in NMC and NCA cathodes are Ni and Co ions and the oxidation of transition metals proceeds by oxidation of Ni^{2+} (NMC) and Ni^{3+} (NCA) to Ni^{4+}, followed by oxidation of Co^{3+} to Co^{4+}. Mn and Al do not participate in the redox reaction and act as structural stabilizers[86].

Here, we categorized the identified structural degradation mechanisms of the NMC/NCA cathodes in three categories as follow; (1) cationic migration and phase transformation[87–90]; (2) oxygen release reaction[91]; (4) Li redistribution and extraction[92]; (4) inter/intragranular cracking and fragmentation[93–95]. A representative figure from each degradation mechanism is shown in Figure 4. It should be emphasized that although these phenomena are casted into distinct groups, their occurrence are highly corelative and often happen as a chain of events[96,97]. Migration of transition metals (Figure 4A) from their octahedral sites into the alternating Li octahedral sites upon excessive Li-deintercalation (increased formation of Li vacancies) and/or temperature rise, is regarded as an initial step in the structural degradation of the NMC/NCA cathodes[89,98]. Such atomic migration triggers the phase transition of the layered ($R\bar{3}m$) structure to the $LiMn_2O_4$-type spinel phase ($Fd\bar{3}m$) and results in oxygen release reaction (Figure 4B)[33,88,99]. TEM investigation on the charged NMC cathodes has shown that Ni is the first cation that migrates to the Li layer and thus has a large contribution on the structural instability of NMC cathodes[87]. In-situ heating STEM/EELS experiments also demonstrated that upon increasing the Ni content, oxygen release and structural degradation are facilitated and occur in lower temperatures[51]. Similarly, in-situ X-ray absorption near edge spectroscopy (XANES) analysis on NCA and NMC cathodes have concluded that Ni is the first cation that undergoes the valence reduction in charged NCA and NMC cathodes[33]. It is also suggested that the migration pathways of Ni and Co to the adjacent Li octahedral sites are different. For instance, although Co ions pass through the nearest neighbor tetrahedral sites to migrate into the octahedral Li sites, the migration of Ni ions into the Li layers does not involve the occupation of the adjacent tetrahedral positions and occurs directly from the transition metal slabs to the Li sites, since Ni ions are not stable in the tetrahedral sites[33,87,100,101]. Although both routes lead to the $LiMn_2O_4$-type spinel phase formation, continued migration of Ni ions into Li octahedral sites will lead to the formation of the MO-type rock-salt ($Fm\bar{3}m$) phase. However, Co atoms prefer to migrate to the Li tetrahedral sites and form Co_3O_4 spinel phase that has a higher oxygen stoichiometry compared to the MO type rock-salt phase[102]. Additionally, employing extended X-ray absorption fine structure (EXAFS) analysis on heated NMC cathode, it was concluded that while local coordination of Ni corresponds to $LiMn_2O_4$-type spinel, local coordination of Co transforms to Co_3O_4 spinel type that is a more stable structure. As such, while $LiMn_2O_4$-type spinel structure around Ni cations transfers to rock salt NiO at 350 °C, transition from spinel Co_3O_4 to rock-salt CoO was not observed up to 500 °C. Furthermore, the formation of pure Ni nano particles at the surface of NCA cathodes during in-situ heating TEM experiments denotes to a higher structural stability around Co sites compared to Ni sites[52]. These explain the underlying reasons for increased oxygen release extent by increased Ni content in the cathode composition. Based on the EXAFS analysis Mn cations' environment is thermally stable up to about 400 °C, which is due to the stability of Mn^{4+} in the octahedral sites that contributes to the stability of NMC structure. AIMD simulation on the single oxygen atoms in NMC structures with various local coordination structure units (LCSU), elucidated that the oxygen atoms that have more Ni in their LCSU are highly unstable, and oxygen atoms in such LCSUs are more prone to break bonds with the transition metals and release as O_2[57]. However, the higher number of Mn atoms in LCSU increases the bonding stability of O-TM drastically. These observations were in accordance with the previously reviewed experimental data suggesting the local instability sequence of Ni >> Co >> Mn in NMC structures[87].

In addition to the chemical composition, particle size and morphology are important factors in determining the thermal stability of NMC and NCA cathodes[33,103,104]. Employing analytical electron microscopy investigations, it has been suggested that subsequent to electrochemical cycling Li deficiency at the surface layer is responsible for O1 phase formation in the outmost surface regions that causes the surface instability of the cathode particles[105]. Also, the presence of the undercoordinated atoms at the surface, and direct contact of cathode surface with the electrolyte are among the reasons for surface instability of cathode materials[106]. Additionally, recent reports clarified that the surface phase transition is facet dependent. Meaning that, due to the higher surface energy and higher concentration of under-coordinated oxygen atoms of some facet terminations, the oxygen release and the phase transitions are more favorable to occur in specific facets[107–109].

Redistribution of Li within the cathode particles has also been observed in the early stages of the thermal decomposition in NMC samples[92], which eventually leads to Li extraction in form of Li-based surface protrusions upon increased duration of high temperature exposure. The Li-based protrusions are in the shape of lumps or whiskers that resemble the morphology of Li-dendrites that grow on Li metal anodes[92]. Cracking and fragmentation of cathode materials are identified as other degradation mechanisms that occur due to the generated strain during the phase transitions and oxygen release reaction[106]. This degradation results in the rapid capacity fade and failure of the battery due to the lost contact and inactivity of the detached particles. The cracking of the cathode particles has been observed in both intragranular regions (inside the single crystal primary grains and particles) and in the intergranular spaces (in the grain boundaries and in between the primary particles), as demonstrated in the Figure 4C and 4D respectively. High cut-off voltage cycling leads to formation of high density of intragranular cracking. It was proposed that, large strain associated with high extent of delithiation/lithiation cannot be accommodated by highly packed primary particles, therefore inhomogeneous mechanical stress applied on each primary grain is released by formation of the dislocations. To reduce the accumulated strain in the dislocation cores, Li and O release from the area (Figure 4C). Therefore, the dislocation cores gradually evolve into premature cracks by further electrochemical cycling. In this condition some of the lattice spacing in (003) direction abruptly increase from 0.48 to about 0.8 nm. Finally, the premature cracks turn into complete cracks that lead to fragmentation and dissociation of the cathode grains[93,95]. Moreover, the intergranular cracking is known be the result of inhomogeneous lattice contraction and expansion in repeated cycling at high cut-off voltages (4.7 V)[94]. Such contraction and expansion of the primary particles will lead to the cracking and disintegration of primary grains and loss of contact of the active materials. It was also suggested that the phase transformation and oxygen release reaction as a result of high temperature exposure could lead to the accumulation of tension stress in the grain boundaries resulting in intergranular cracking (Figure 4D)[106,110].

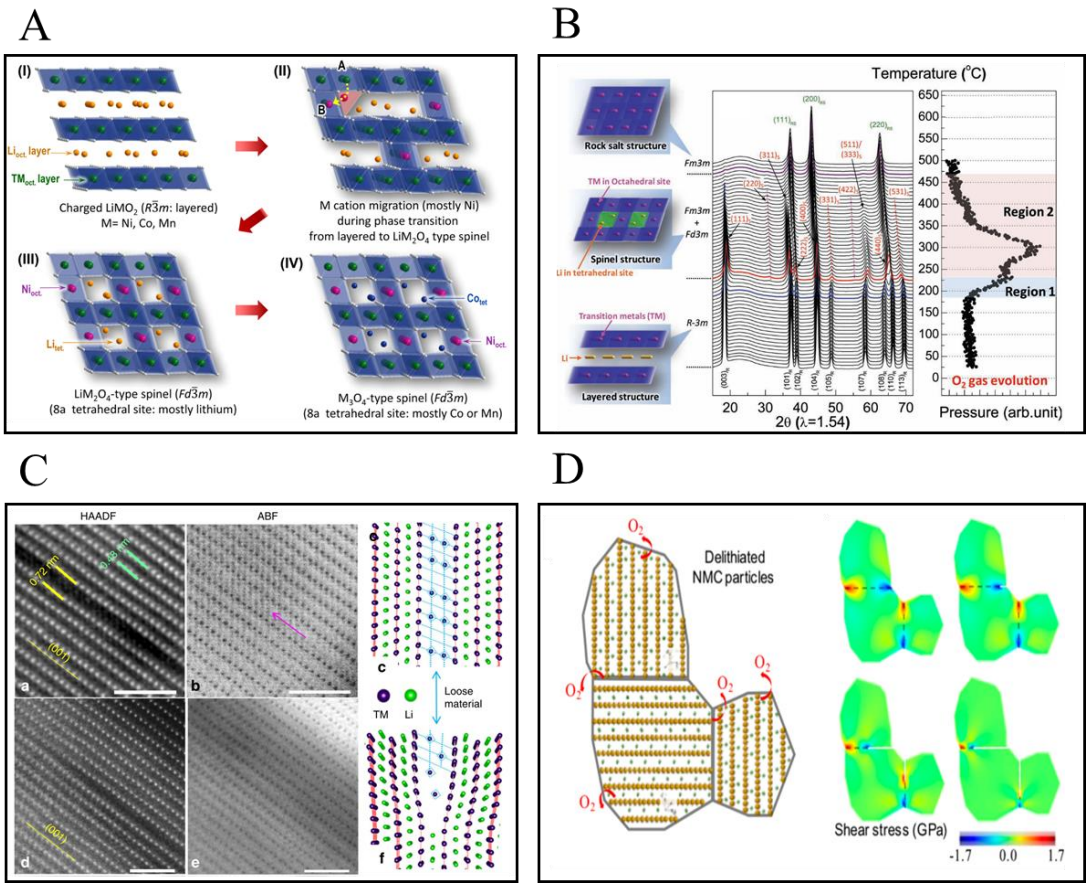

Figure 2. Demonstration of NMC/NCA structural degradations and oxygen release mechanisms. (A) Schematic illustration of cationic migration and structural reconstruction: Reproduced with permission.[103] Copyright 2014, American Chemical Society. **(B)** Time resolved X-ray diffraction/mass spectroscopy (TRXRD-MS) results correlating the structural reconstruction to the oxygen release phenomenon: Reproduced with permission.[33] Copyright 2012, Wiley-VCH. **(C)** Atomic resolution image of intragranular crack formation in overcharged NMC structure: Reproduced with permission.[93] Copyright 2017, Nature Publishing Group. **(D)** Finite element modeling of sheer stress in the grain boundaries of NMC cathodes leading to the intergranular cracking of cathode particles: Reproduced with permission.[110] Copyright 2018, American Chemical Society.

2.2. Spinel Structured Cathodes

Reversible Li intercalation in the spinel phase $A(B_2)X_4$ compounds was discovered by Thackeray and Goodenough[111]. In these compounds, A and B refer to the cations in the tetrahedral (8a) and octahedral (16d) sites in a cubic ($Fd\bar{3}m$) structure respectively, and X anions that form a cubic close packed structure occupy 32e sites. In this structure, only 1/8 and 1/2 of interstitial tetrahedral and octahedral sites are occupied by A and B cations, which enables unrestricted shuttling of Li ions through the vacancies[112,113]. Spinel phase cathodes are one of the main candidates for the next generation of large scale energy storage systems, due to the relatively high energy density (607 W h Kg^{-1}), high ionic and electronic conductivity (10^{-6} and 10^{-4} S cm^{-1} respectively), cost effectiveness (~10 \$ kg^{-1}) and non-toxicity[114]. The main challenge limiting the widespread use of these cathode materials is the rapid capacity fading, particularly at elevated temperatures[115–117]. Mn dissolution, activated by Jahn-Teller distortion of Mn ions at the surface of charged LMO particles, and subsequent deposition on the negative electrode surface, is known as the origin of

this problem (Figure 5A)[115]. The Mn dissolution is also associated with the parasitic oxygen release reaction[118]. Upon charging, LMO structure is destabilized and structural distortion leads to the Mn_3O_4 phase formation. This phase transition is associated with the oxygen release and formation of soluble Mn^{2+} ions (Figure 5B)[118]. Slight increase in the temperature rapidly increases the rate of Mn dissolution and correlative oxygen release. Under such conditions, structural transformation of spinel $LiMn_2O_4$ to the distorted structure and finally to the layered Li_2MnO_3 like (C2m) structure will occur, as identified by atomic resolution STEM imaging (Figure 5C)[119]. Nonetheless, spinel cathodes has a higher thermal stability compared to the layered oxide cathodes, and the release of oxygen has a higher onset temperature of □ 375 °C in de-lithiated $Li_xMn_2O_4$ cathodes[114].

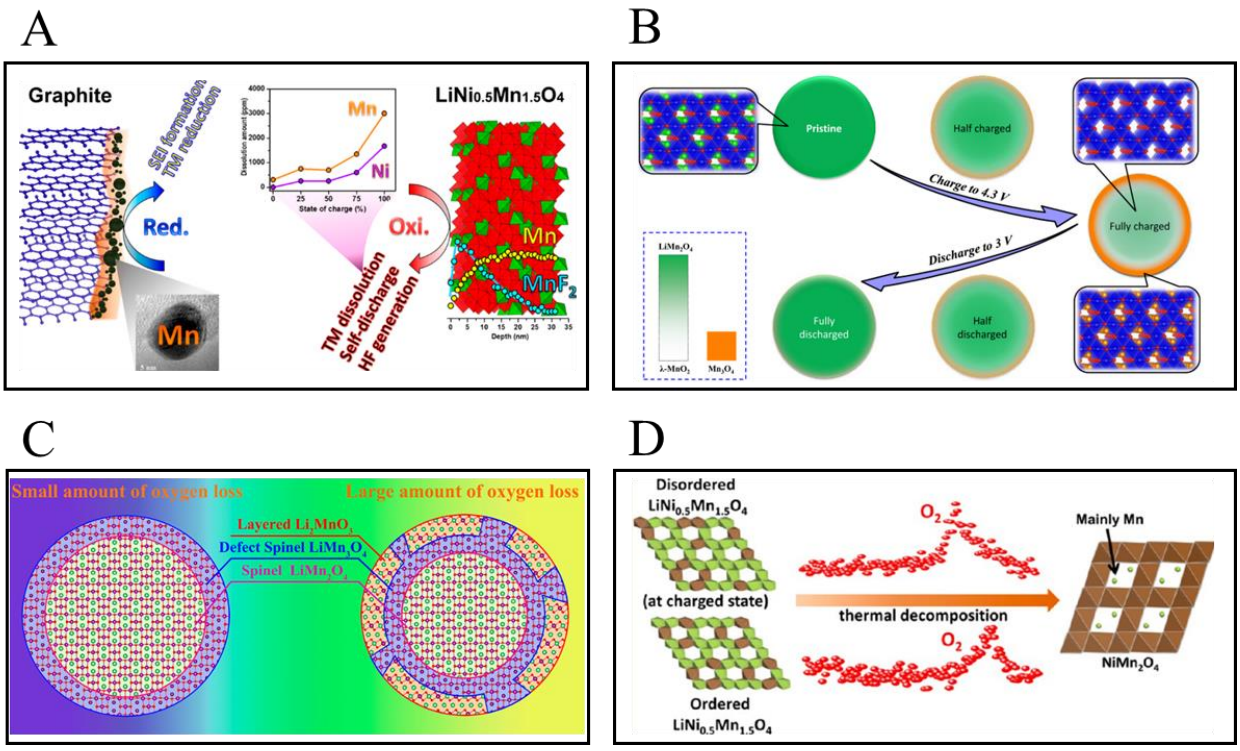

Figure 3. Schematic demonstration of the oxygen release and correlated structural degradations in the spinel phase cathodes. (A) Schematic demonstration of the mechanism of Mn dissolution from LMO cathodes: Reproduced with permission.[115] Copyright 2013, American Chemical Society. **(B)** Partially reversible formation of Mn_3O_4 phase at the surface of LMO cathodes accompanied by oxygen release reaction: Reproduced with permission.[118] Copyright 2014, American Chemical Society. **(C)** Schematic demonstration of the effect of cut-off voltage/thermal decomposition temperature on the extent of oxygen release and sequence of phase transition in the spinel LMO cathode: Reproduced with permission. [119] Copyright 2017, American Chemical Society. **(D)** Higher O_2 release onset temperature of the ordered LNMO spinel cathodes that demonstrates the superior thermal stability of ordered structure compared to the disordered structure: Reproduced with permission. [120] Copyright 2014, American Chemical Society.

Another member of the spinel cathodes family is $LiNi_xMn_{2-x}O_2$ (LNMO), which has a higher operating voltage (4.7 V vs Li/Li^+) and alleviated Mn dissolution issue. However, unlike $LiMn_2O_4$ that is thermally stable up to 375 °C, oxygen release can occur below 300 °C in charged LNMO cathodes[120]. This is due to the presence of highly unstable Ni ions in this structure. Depending on the synthesis annealing temperature, Mn^{4+} and Ni^{2+} distribution in the LNMO crystal structure can

have short-range order, or the Ni and Mn cations can be randomly distributed (long range order). Such structural variations affect the thermal stability of spinel LNMO cathodes. The LNMO cathodes with long range order have demonstrated a superior thermal stability compared to the short range ordered structures (Figure 5D)[120].

2.3. Olivine Structured Cathodes:

Olivine structured cathode materials with the composition of $LiMPO_4$ (M=Ni, Co, Mn, Fe) were developed as safe alternatives for the layered oxide cathodes[121,122]. It is believed that the tetrahedral $(PO_4)^{3-}$ anions have a very strong covalent P-O bonds that do not allow for oxygen release upon exposure to high temperatures[123]. $LiFePO_4$ is known as a very safe and thermally stable cathode material[124] that has been commercialized for EV applications due to high capacity (□170 $mAhg^{-1}$), flat potential profile through the charge discharge process (caused by first order reaction during the redox process), very high thermal stability (600-700 °C)[123], earth crust abundant constituent and low toxicity of the raw materials. However, because of the sluggish kinetics of Li ion transfer, poor electrical conductivity and low operating voltage, scientific efforts have been stirred towards other phosphate cathodes such as $LiCoPO_4$ and $LiMnPO_4$[125–127]. Despite the structural similarities, these cathodes show a very different thermal stability characteristic. As such, thermal analysis and in-situ XRD results demonstrate that while $LiFePO_4$ is thermally stable at a wide range of Li fraction, Li_xCoPO_4 and Li_xMnPO_4 decompose and release oxygen when exposed to elevated temperatures[123,128]. Therefore, it is noted that the constituent transition metals play an important role in defining the thermal stability of the olivine cathode materials. Through high-throughput ab-initio molecular dynamics and first principle calculations[122,129], it has been concluded that the ligand field theory (LFT) is governing the thermal stability of the olivine structured cathode materials. This means that the half-filled high spin electronic configuration that consists of five parallel spin electrons is a highly stable configuration for transition metals in olivine structures. Therefore, when $LiFePO_4$ is in its delithiated state ($FePO_4$), Fe ions with a valence state of 3^+ have a stable half-filled high spin configuration that stabilizes the structure. Nevertheless, Co and Mn phosphates have six and four electrons in their valence orbitals at charged state, respectively. This is an unstable configuration and results in their valence reduction at high temperatures[129]. In fact, high-throughput density functional theory (DFT) calculations have shown that thermal decomposition onset temperature of some specific olivine cathodes can be lower compared to their layered oxide counterparts[122]. Their findings suggest that there is a trade-off between the intercalation voltage and thermal stability of these class of cathodes. Therefore, a high voltage Li-ion intercalation reaction in $LiMnPO_4$ and $LiCoPO_4$ results in a very unstable delithiated structures.

2.4. Li-Rich Cathodes:

Li-rich NMC cathodes that are discovered by partial cationic substitution of transition metals with extra Li ions in layered oxide cathodes, are considered as the next milestone in the advancement of the positive electrodes in the Li-ion batteries[130]. Li-rich cathodes that can achieve capacities greater than 250 $mAhg^{-1}$ when cycled between 2-4.8 V (Figure 6A)[131–133] have a complex crystal structure denoted in three opposing ways: (1) a solid solution with the original ($R\bar{3}m$) layered structure, where some of the extra Li ions are occupying the transition metal sites[134]; (2) a nano-composite of the C2/m Li_2MnO_3 and the $R\bar{3}m$ $LiMO_2$ with the general formula of xLi_2MnO_3-(1-x)$LiMO_2$[135,136], known as Li-Mn rich (LMR) cathodes; (3) a single phase solid solution C2/m Li_2MnO_3 phase with random Li/TM mixture (Figure 6B)[137]. Despite the favorable high capacity, the industrial utilization of the so-called Li-rich cathodes is not realized due to poor capacity

retention, voltage fade and low Columbic efficiency[138–141]. In general, the two-step plateau that is observed in the voltage profile of Li-rich cathodes has been explained by the participation of oxygen species in the electrochemical reaction known as the anionic redox reaction[142]. The anionic redox reaction eventually results in the release of lattice oxygen and transition metal migration, which leads to the structural evolution, cracking, capacity and voltage fade issues[143–146].

Employing DFT calculations, it has been understood that due to formation of Li-O-Li bonds that only exist in the Li-rich cathodes, density of states (DOS) increases near the Fermi level of oxygen ions (Figure 6C) and results in evolution of labile electrons. Since there is a large energy gap between O 2p orbitals and Li 2s orbitals, these labile electrons are unhybridized, so their energy level is not dependent on the cationic redox reaction[147]. Therefore, anionic redox can occur simultaneously or subsequent to the cationic redox reaction depending on the electronic band structure of the metal cations. Anyhow, labile oxygen electrons can hybridize with other oxygens, forming O-O dimers[148]. The oxygen dimerization that has a low kinetic barrier results in the formation and release of molecular O_2 and irreversible transition metal migration into Li vacancies[149]. The formation of O-O dimers occurs only when oxygen atoms rotate to overlap their orbitals, which requires broken metal-oxygen bonds[142,150,151]. As such, it is suggested that the degree of cation-anion covalent bonding is a key parameter in stabilizing the structure and retaining the reversibility of the anionic redox reaction. Hence, Li-rich cathodes containing 4d transition metals such as Li_2RuO_3 have been proposed for stabilized oxygen redox reaction[134,152]. These structures show a superior structural stability and less gas release compared to 3d-tranistion metal Li-rich NMC cathodes, but at the expense of significantly higher material cost. It is also suggested that the substitution of inactive ions such as Mn^{4+} with electrochemically active ions (e.g. Ru^{+}), to fully compensate for the Li^{+} charge transfer, alleviates the anionic charge compensation and stabilizes the structure[50]. On the other hand, another research based on Raman spectroscopy claimed that the O-O vibration that is presents in peroxo-like $(O_2)^{n-}$ species were not observed in the charged Li-rich cathodes indicating that O-O dimers were not formed during the cycling[43]. Instead, based on resonance inelastic X-ray spectroscopy (SIXS) analysis it was concluded that, upon charging the Li-rich cathodes to over 4.5V, electron holes are formed on the oxygen atoms that are locally coordinated with Mn^{4+}/Li^{+} ions. Electron hole formation over these O atoms destabilize their ionic bonds with the local Mn^{4+}/Li^{+}, which results in the oxygen release and structural degradation of the cathodes. Moreover, utilizing atomic resolution imaging, it has been shown that due to the loss of excess Li ions upon electrochemical cycling of Li-rich cathodes, monoclinic (C2/m) structure transforms to hexagonal ($R\bar{3}m$) phase, which then evolves into the spinel ($Fd\bar{3}m$) structure (Figure 6D)[153]. Such monoclinic to spinel phase transition accounts for the voltage decay that is normally observed in Li-rich cathodes and accompanies the oxygen release reaction. This phase transition can also lead to cracking and fragmentation of the cathode particles that further deteriorates the capacity[96,154].

Thermal decomposition of the Li-rich cathodes is studied and compared with their conventional layered oxide counterparts. Thermal decomposition of the Li-rich cathodes occurs at around 190° C for the half charged $Li[(Ni_{0.5}Mn_{0.5})_xCo_y(Li_{1/3}Mn_{2/3})_{1/3}]O_2$ (x + y = 2/3, y = 1/12 and 1/6) electrodes[155]. However, by charging the cathode to the second plateau where anionic redox reaction is activated, the onset temperature for the exothermic reaction between the cathode and the electrolyte decreases to around 130° C. This is significantly lower than the thermal decomposition temperature of conventional layered oxide cathodes[156]. This is due to the presence of readily oxidized Li-O-Li bonds in Li-rich cathodes, which facilitates the thermal

decomposition/oxygen release and decreases the onset temperature of the decomposition of charged Li-rich cathodes. Despite the lower onset temperature of thermal decomposition, the amount of released oxygen is relatively smaller for Li-rich cathodes compared to their conventional layered counterparts[157,158]. This is attributed to the dissimilar phase transition route of the Li-rich and conventional layered oxide cathodes upon thermal decomposition. Although, the $LiNi_{0.8}Mn_{0.1}Co_{0.1}O_2$ sample transforms from the layered phase to the spinel and then to the rock-salt phase, the Li-rich structure only transform to the spinel phase and then the spinel phase remains stable throughout the thermal treatment process. This difference is due to higher tendency of Ni ions in forming the rock-salt structure as opposed to highly stable Mn ions. Additionally, it has been demonstrated that the sequence and onset of such phase transitions is also dependent on the utilized electrolyte[159].

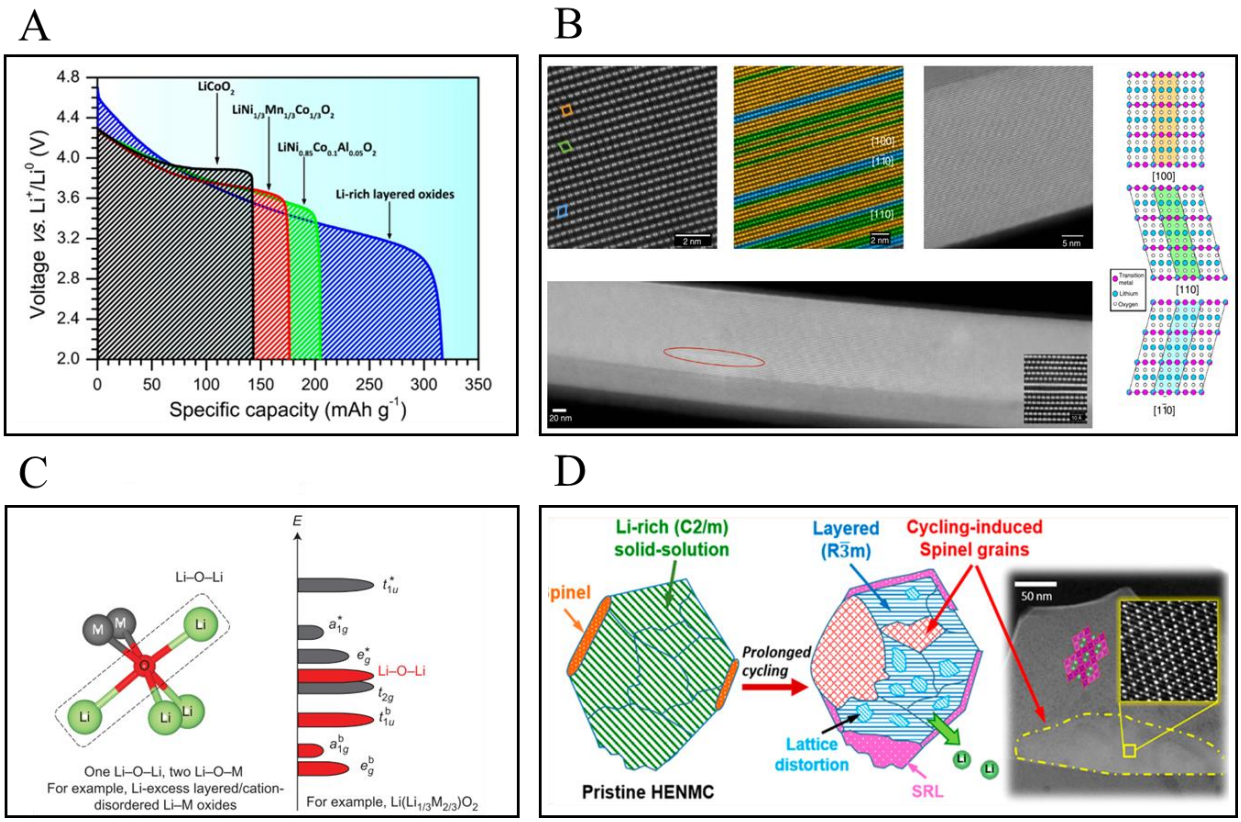

Figure 4. Depiction of the differences in the capacity, redox reaction and degradation mechanism of Li-rich cathode materials compared to conventional layered oxide cathodes. (A) Comparison of voltage profile and electrochemical capacity of the layered oxide cathodes: Reproduced with permission. [132] Copyright 2017, American Chemical Society. **(B)** Atomic resolution image showing a single phase monoclinic (C2/m) structure of a Li-rich cathode particle: Reproduced with permission. [137] Copyright 2015, Nature Publishing Group. **(C)** Schematic of local atomic coordination and electron band structure of Li-excess cathodes, that enables the anionic redox reaction: Reproduced with permission.[147] Copyright 2016, Nature Publishing Group. **(D)** schematic demonstration of the identified phase transition sequence and structural degradation of Li-rich cathodes: Reproduced with permission. [153] Copyright 2018, American Chemical Society.

3. Strategies to Improve the Structural stability of the Cathodes

3.1. Chemical Composition Modification:

Oxygen release reaction and structural instability of the cathode materials are heavily dependent on the chemical composition of the cathode materials. DFT modeling have demonstrated that the energy of oxygen vacancy formation is a function of the type of transition metal species that are locally bonded with each oxygen atom[57]. As such, modification of the chemical composition of the cathodes have been considered as a promising solution for improving the thermal and structural stability of the cathode materials. In this review, research efforts focused on chemical composition modification as an approach to improve the structural stability of the cathode materials have been summarized in 3 categories; (1) doping; (2) chemical gradient compositions; (3) core shell structures (Figure 7).

3.1.1. Doping. Doping and cationic substitution of transition metals is one of the most widely explored approaches in improving the structural stability of the cathode materials. As such, the effect of the monovalent cations such as K and Na[160–167], divalent ion dopants such as Mg and Zn[168–175], trivalent Fe, Al and Au dopants[145,176–193], and tetravalent cations such as Ti and Ru[194–201] have been studied on the structural stability of various cathode materials. It has been demonstrated that dopants with various valence groups can affect the structure and the properties of the cathode materials in different ways. For instance, it is realized that monovalent and divalent dopants occupy the Li sites in the cathodes structures[202]. Therefore, due to the electrochemical inactivity of the mono and divalent dopant elements throughout the cycling, they remain in the Li slabs acting as pillars that uphold the structural integrity. This phenomenon is known as the "pillar effect". Also, the presence of the dopants in Li sites reduces the chances of Li trivacancy formation, hindering the transition metal migration and oxygen release in the delithiated cathodes[203,204]. In addition, it is suggested that dopant ions larger than Li^+ increase the lattice spacings and allow for faster Li-ion diffusion with lower activation energy, thus enable high rate cycling and alleviate structural degradation. Moreover, doping the Li sites with divalent ions such as Mg increases the average charge on the Li sites that decreases the charge on the metal sites, alleviating the lattice distortion and improving the structural stability[205]. Substituting 10% of Co cations with Al is shown to be promising in stabilizing the structure resulting in □100 °C delay in the thermal decomposition of NMC cathodes [185,206]. Such observation is explained by higher stability of Al ions in the intermediate tetrahedral sites that increases the energy barrier for migration of transition metals and promotes the structural stability[190,191]. Similarly, addition of Fe^{3+} to the spinel LMNO cathodes have shown to improve the thermal stability by alleviating the oxygen release reaction. This is linked to the preferred migration of Fe cations from octahedral sites to Li tetrahedral sites, which stabilizes the Fe_3O_4 type spinel and hinders the oxygen release reaction upon high temperature exposure[145]. In general, trivalent and tetravalent dopants that occupy the TM sites increase the lattice spacings, reduce the bandgap, and increase the electrical conductivity of the cathodes. In addition, through DFT calculations, it was demonstrated that Sb^{3+} doping alters the density of states[189,207]. In this case, the charge around O atoms become more negative in presence of the Sb dopants, which can stabilize the lattice oxygen during electrochemical extraction of Li ions (Figure 7A)[189].

In addition to cationic substitution, doping of oxygen sites with anions such as F, Cl and S has been carried out in the recent years. Fluorine doping of oxygen sites in Li-rich layered oxide cathodes was shown to improve the structural stability and delay the oxygen release reaction for

□20°C[208,209]. However, a recent DFT study has shown that anionic doping could have conflicting effects on various properties of the cathodes[210]. It has been demonstrated that while F can mitigate Ni migration and improve the cycling stability, it will promote Li/Ni cationic mixing in the synthesis process. On the other hand, while Cl and S alleviate the Li/Ni mixing issue, they adversely affect the structural stability of the cathodes when doped into O sites[210]. Moreover, simultaneous doping of cationic and anionic sites, known as co-doping, is another strategy to improve the structural stability of the oxide cathodes that has been utilized in some of the recent works and should be further explored[211–213].

3.1.2. Chemical Concentration Gradient. Another novel approach in designing durable cathode structures without compromising their capacity is the synthesis of chemical concentration gradient cathodes. In these structures, while the core of particles is rich in high capacity elements such as Ni, the structural stability is achieved by increasing the content of the electrochemically stable elements such as Mn at the surface (Figure 7B)[214]. Thus, the stable Mn-rich surface protects the high capacity Ni-rich core from structural degradation and oxygen release, while maintaining the overall energy density of the material [215–223].

3.1.3. Core-shell Composition. Since many unwanted side reactions as well as oxygen release initiate at the cathodes surface, modification of chemical composition of the surface regions without affecting the bulk composition has also been pursued to improve the structural integrity of the cathodes. In this context, incorporation of stabilizing elements such as Al, Zr and Mn in a thin outer layer of cathode particles was suggested to improve the structural stability of $LiCoO_2$ samples[224–229]. Such core-shell structures are generally obtained by coating the cathode particles with a metal containing composition, followed by a thermal treatment that allows for diffusion of coating element into the cathode structure[230]. Additionally, synthesis of dual phase core-shell cathodes is another approach in improving the structural stability of the cathode materials[231]. For instance, by forming a layer of spinel $LiMn_2O_4$ on a layered Ni rich cathode materials, capacity fading and oxygen release could be mitigated[232]. Moreover, formation of an oxygen-lithium deficient shell was shown to stabilize the structure of Li-rich cathodes. It was illustrated that by uniform distribution of oxygen vacancies at the surface of Li rich NMC cathodes, higher cycling stability and reduction in the release of oxygen at high voltages can be realized (Figure 7C)[233].

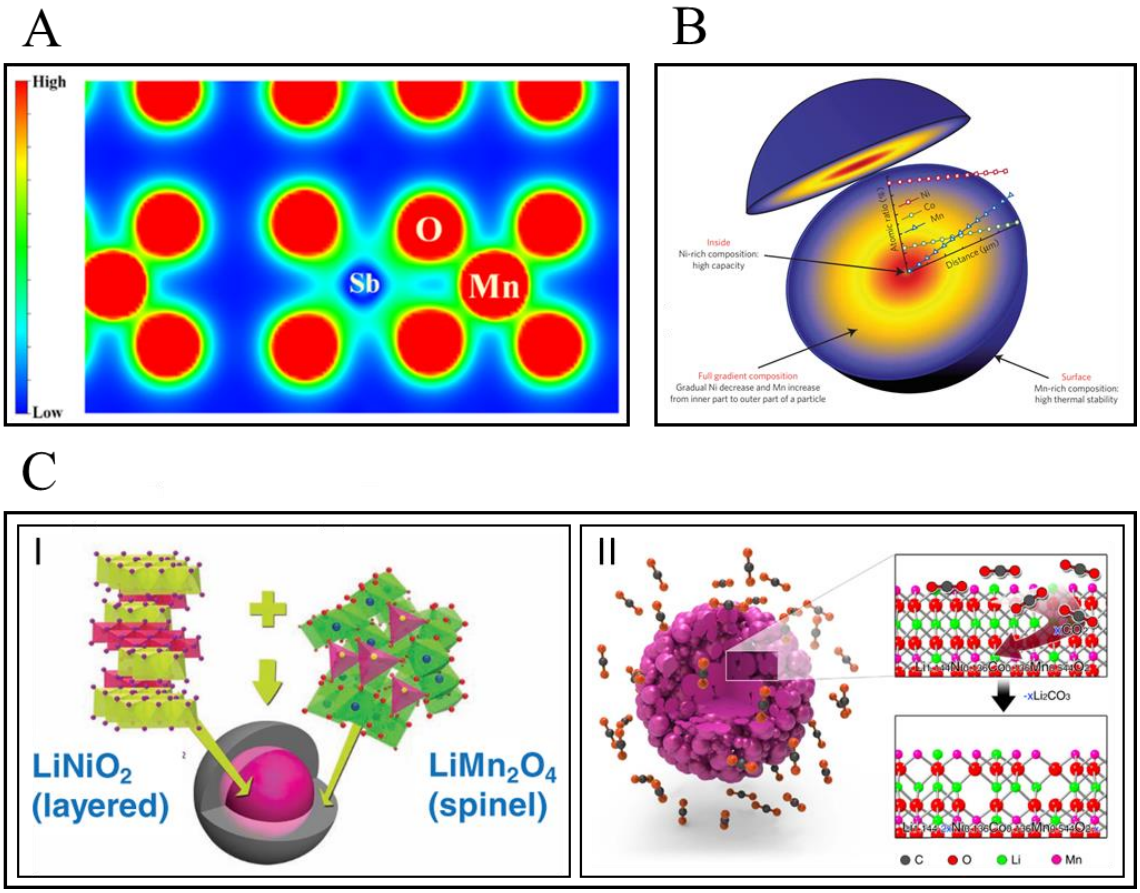

Figure 5. Schematic representation of the chemical composition modification approaches used to improve the structural stability of the cathode materials. (A) Atomic structure of a cationic doped layered oxide cathode: Reproduced with permission.[189] Copyright 2018, American Chemical Society. **(B)** Schematic illustration of a chemical concentration gradient cathode: Reproduced with permission. [214] Copyright 2012, Nature Publishing Group. **(C)** Schematic figures representing core-shell cathode structures: Reproduced with permission. [232] Copyright 2011, Wiley-VCH. [233] Copyright 2016, Nature Publishing Group.

3.2. Coating Strategies:

Prominent progress in stabilizing the structure of the cathodes and improving their thermal stability were achieved by coating approaches. Since the first breakthrough in improvement of the thermal stability of cathodes, achieved by Cho *el al.*[234], several research groups have investigated the surface coating for hindering the oxygen release reaction and improving the structural stability of cathode materials. Herein, we have categorized the surface coating approaches based on the utilized coating material and will review the mechanisms by which the structural stability is improved in different articles.

3.2.1. Phosphate Coating. Aluminum phosphate is the first coating material that was successfully utilized to prevent the thermal runaway reaction in $LiCoO_2$[234]. In this report, it was shown that by charging a pouch cell containing $LiCoO_2$ and liquid electrolyte to 12 V, the cell will experience the thermal runaway reaction and eventually catch fire. However, no indication of thermal runaway and catastrophic failure was detected by exposing the $AlPO_4$ coated $LiCoO_2$ electrode to the same condition. Later on, thickness optimization and identification of the mechanism of retarding the thermal runaway reaction was carried out[235–237]. Utilizing XPS and STEM characterization techniques, it was explained that during annealing, $AlPO_4$ coating on the surface breaks into Li_3PO_4 and $LiCo_{1-x}Al_xO_2$ phases. Formation of Li_3PO_4 that is a lithium conducting phase, reduces the potential at the surface and thus higher structural stability can be achieved in over-charging conditions[237]. Moreover, it was also suggested that the decomposition of $AlPO_4$ and penetration of the Al into the surface of $LiCoO_2$ is contributing to higher structural stability of the coated cathodes (Figure 8A)[238]. Recently, ALD deposition of $AlPO_4$ layer that allows for a controlled deposition of the coating layer was achieved[239]. Subsequent to the utilization of aluminum phosphate coatings, the effect of other metal phosphate coatings such as $FePO_4$[240], Li_3PO_4[241–244], $LiMnPO_4$[245], $PrPO_4$[246] and $LiMgPO_4$[247] on the structural stability of the cathodes were explored. Similar to $AlPO_4$, coating of $LiMgPO_4$ was demonstrated to decompose during the calcination process. The decomposition allows for doping the inactive Mg^{2+} into the Li sites at the surface of particles that activates the "pillar effect" during the electrochemical cycling. The remaining phosphate phase inhibits the parasitic oxygen release and other side reactions at the surface of the Li-rich cathode particles leading to improved voltage stability and capacity retention of the battery.

3.2.2 Oxide Coating. Parallel to the advancements in utilizing phosphate coatings, researchers explored the effect of oxide coatings on the O_2 release and structural stability of cathode materials. In this approach, magnetron sputtering and atomic layer deposition are the heavily used techniques for deposition of the oxide coatings. In the early investigations, it was observed that the metal oxide coatings such as Al_2O_3 and MgO delay the thermal decomposition reaction and reduce the magnitude of the parasitic exothermic reaction of cathode/electrolyte[248]. Later on, it was demonstrated that a thin coating layer of alumina can greatly enhance the electrochemical and thermal stability of $LiCoO_2$[249,250]. To understand the mechanism of structural stabilization achieved by such oxide coatings, researchers have utilized DFT and ab-initio molecular dynamics calculations to show how the thermal decomposition and oxygen evolution reaction are inhibited by the oxide coatings[251], and also how Li-ions transfer through such coatings[252,253]. It was observed that during electrochemical cycling, Al_2O_3 coating layer is gradually lithiated. Ultimately, the alumina coating transforms to the thermodynamically favorable composition of $Li_{3.4}Al_2O_3$[252]. After reaching to this stable composition, $Li_{3.4}Al_2O_3$ conducts the Li-ions to the cathode structure. Interestingly, first principle calculations also demonstrated that the oxygen release from the cathode can only be suppressed by the lithiated phase of Al_2O_3, which forms naturally when the alumina coated cathode particles are cycled (Figure 8B)[251]. Moreover, employing advanced characterization tools such as STEM-EELS, researchers could demonstrate that Al_2O_3 coating can suppress the reduction of transition metal cations at the surface of the cathode particles, which denotes to the suppression of the oxygen release from the cathode surface[254–256]. It was also demonstrated that, upon alumina coating of $LiCoO_2$, a portion of Al from the coating layer diffuses to the surface layer of the cathode. The Al doped $LiCoO_2$ structure is a more stable surface and hinders the oxygen release[257]. Moreover, the contribution of many other metal oxide coatings such as TiO_2[258–260], ZnO[261–264], MgO[248,265] and many more[266–275] are studied on the structural stability of cathode materials. For instance, Cheng *et al.*[276] have compared the performance of Al_2O_3 versus TiO_2 coating on $LiCoO_2$ and have suggested that Al_2O_3 coated cathode has a superior electrochemical performance. They attributed these observations to the difference in the band gap of the coating materials and showed that smaller band gap of TiO_2 results in its participation in the redox reaction and triggering unwanted side reactions. Accordingly, it was suggested that for $LiCoO_2$, the band gap of the coating material should be larger than 3.9 eV. Therefore, MgO coating with 7.8 eV band gap would make a good protective coating for $LiCoO_2$[277].

3.2.3. Other Coating Strategies. Aside from phosphate and oxide coatings, the effect of the other coating materials such as polymers[278–280], fluoride coatings[281–285] and two dimensional materials [286] on the structural stability of the cathodes have been explored. Fluoride coatings deposited through ALD technique have been shown to enhance the cycling and structural stability of oxide cathodes under high rate and high voltage cycling conditions. For instance AlF_3 is suggested to prevent the formation of LiF at the surface of the cathodes, thus preventing the impedance rise and Co dissolution[283]. Moreover, $LiAlF_4$ that is shown to be a highly stable compound with high electrical and ionic conductivity was suggested to significantly improve the surface stability of the Ni-rich NMC cathodes[282]. Polymer coating is another strategy for improving the structural stability of oxide cathodes. Conductive polymer coatings are either applied directly to the surface of cathode particles[287], or employed as a double layer on the oxide and sulphate coating layers[288,289]. Similar to many coating approaches, conductive polymer coatings are suggested to provide a stable interface layer preventing electrolyte side reactions and metal dissolution. Owing to the recent progress in the synthesis of 2D materials and comprehensive understanding of their properties, encapsulation of cathode particles by two-dimensional materials such as graphene and its derivatives are being pursued by researchers. Ultra-thin layers of reduced graphene oxide was firstly used as highly conductive pathways for improving the conductivity of $LiFePO_4$ electrodes[290–292]. Recently, conformal wrapping of reduced graphene oxide (rGO) layers around cathode particles was enabled by employing silane coupling agents[293]. Using such methodologies, facile and scalable coating of highly conductive and chemically inert rGO layers have been achieved that led to improved ion conduction kinetics throughout the electrodes (Figure 8C). Also structural stabilization of cathodes due to excellent chemical stability of the rGO coating layers is realized by utilizing by graphene-encapsulation of cathode particles[293–295].

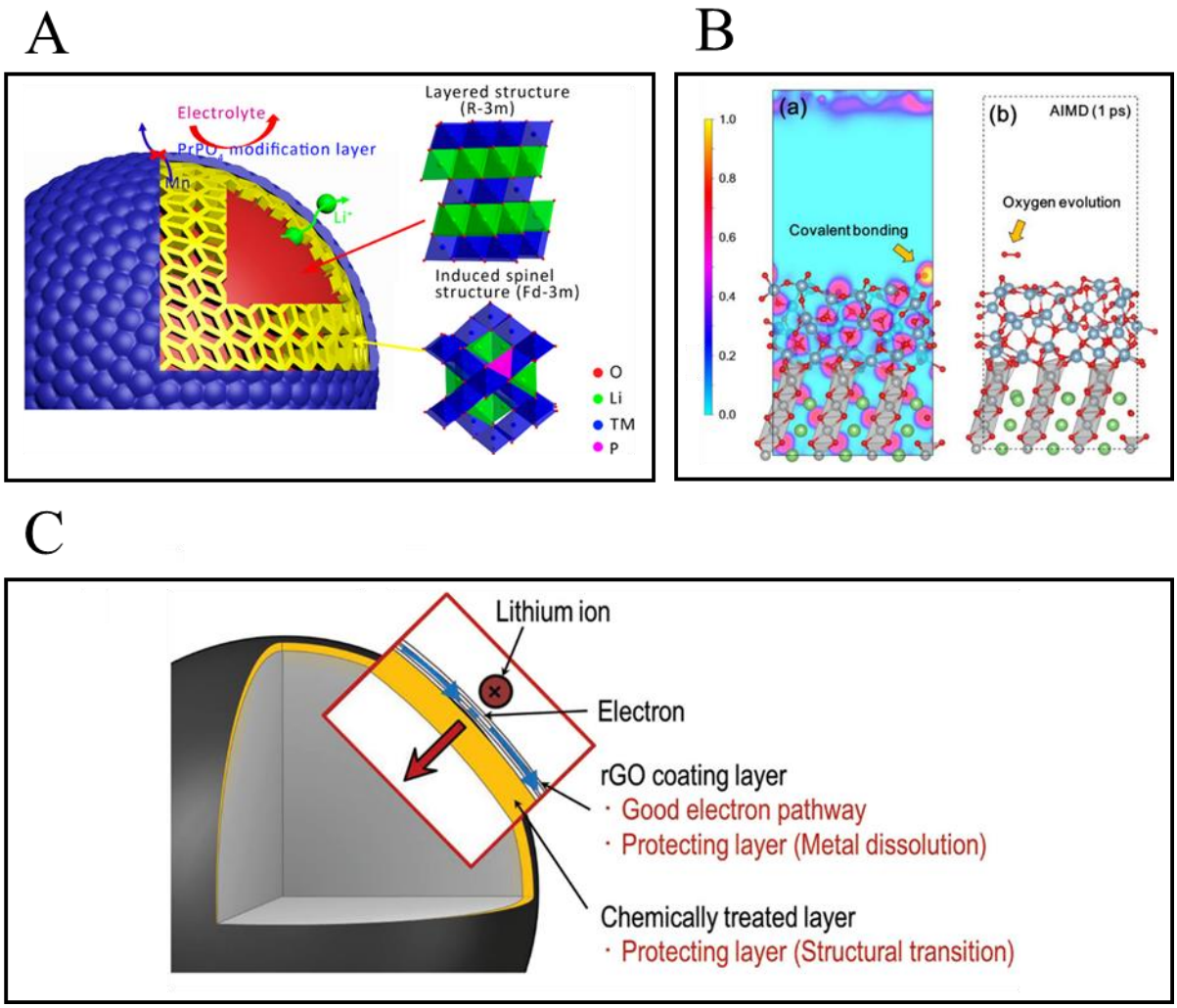

Figure 6. Schematic illustration of coating strategies utilized to improve the structural stability of cathodes. (A) Schematic representation of phosphate coating on layered oxide cathode particles: Reproduced with permission. [246] Copyright 2017, American Chemical Society. **(B)** Representative AIMD modeling results on the effect of alumina coatings on oxygen release and structural stability of layered oxide cathodes: Reproduced with permission. [251] Copyright 2015, American Chemical Society. **(C)** Schematic representation of the rGO coating and its effects on the physical properties of the cathode materials: Reproduced with permission. [295] Copyright 2014, Wiley-VCH.

Summary and Future Prospective:

The oxygen release reaction and the correlated structural degradation mechanisms of the cathode materials are not only detrimental to the service life of the Li-ion batteries but also cause the catastrophic failure and thermal runaway events. Herein, we reviewed the recent progress in understanding and mitigating the parasitic oxygen evolution and the correlated structural degradation of the major cathode materials. In summary, oxygen release is a complex, multimodal reaction that occurs under diverse abusive conditions and is influenced by many parameters such SOC, size and morphology, chemical composition, and atomic arrangements of the cahodes. O_2 release phenomenon is identified at the surface of the cathode particles as characterized by the valence state reduction and structural reconstruction, as well as the bulk of the cathode particles,

identified by defect formation and inter/intragranular cracking. The efforts to suppress such detrimental reactions can be categorized in two main approaches: (1) surface coating and (2) chemical composition modification. Coating approaches have shown to be highly effective in suppressing the oxygen release and mitigating the thermal runaway of LIBs. However, it is still not clear that if surface engineering approaches can hinder the bulk-originated oxygen release mechanisms and control the cracking and disintegration of cathode materials. In addition, due to inhomogeneous expansion and contraction in the cathode/coating interface during the electrochemical cycling, the coated and core-shell cathodes are highly prone to delamination and mechanical failure during repeated cycling. On the other hand, chemical composition modification approaches can effectively suppress the oxygen evolution reaction both at the bulk and the surface level. However, doping and alloying of cathode materials are associated with challenges such as uniformity of the dopant dispersion and electrochemical properties deterioration by the introduction of the inactive dopant ions.

Acknowledgments

R. Shahbazian-Yassar acknowledges financial support from the National Science Foundation (Award No. DMR-1620901). J. Lu and K. Amine gratefully acknowledge support from the U. S. Department of Energy (DOE), Office of Energy Efficiency and Renewable Energy, Vehicle Technologies Office. Argonne National Laboratory is operated for DOE Office of Science by UChicago Argonne, LLC, under contract number DE-AC02-06CH11357.

References:

[1] J.-M. Tarascon & M. Armand, *Nature* **2001**, *414*, 359.
[2] K. M. Abraham, *J. Phys. Chem. Lett.* **2015**, *6*, 830.
[3] L. Lu, X. Han, J. Li, J. Hua, M. Ouyang, *J. Power Sources* **2013**, *226*, 272.
[4] J. B. Goodenough, K. S. Park, *J. Am. Chem. Soc.* **2013**, *135*, 1167.
[5] N. Nitta, F. Wu, J. T. Lee, G. Yushin, *Mater. Today* **2015**, *18*, 252.
[6] Ganesh Venugopal, *J. Power Sources* **2001**, *101*, 231.
[7] Y. Di Zhang, Y. Li, X. H. Xia, X. L. Wang, C. D. Gu, J. P. Tu, *Sci. China Technol. Sci.* **2015**, *58*, 1809.
[8] M. S. Whittingham, *Chem. Rev.* **2004**, DOI 10.1021/cr020731c.
[9] Z. Gong, Y. Yang, *Energy Environ. Sci.* **2011**, DOI 10.1039/c0ee00713g.
[10] R. Jung, P. Strobl, F. Maglia, C. Stinner, H. A. Gasteiger, *J. Electrochem. Soc.* **2018**, *165*, A2869.
[11] Q. Wang, P. Ping, X. Zhao, G. Chu, J. Sun, C. Chen, *J. Power Sources* **2012**, *208*, 210.
[12] N. Williard, W. He, C. Hendricks, M. Pecht, *Energies* **2013**, *6*, 4682.
[13] X. Liu, D. Ren, H. Hsu, X. Feng, G. L. Xu, M. Zhuang, H. Gao, L. Lu, X. Han, Z. Chu, J. Li, X. He, K. Amine, M. Ouyang, *Joule* **2018**, *2*, 1.
[14] R. Spotnitz, J. Franklin, *J. Power Sources* **2003**, *113*, 81.
[15] Y. Saito, K. Takano, A. Negishi, *J. Power Sources* **2001**, *97*, 693.
[16] K. Liu, Y. Liu, D. Lin, A. Pei, Y. Cui, *Sci. Adv.* **2018**, DOI 10.1126/sciadv.aas9820.
[17] Q. Wang, P. Ping, X. Zhao, G. Chu, J. Sun, C. Chen, *J. Power Sources* **2012**, *208*, 210.
[18] D. Aurbach, A. Zaban, Y. Ein-Eli, I. Weissman, O. Chusid, B. Markovsky, M. Levi, E. Levi, A. Schechter, E. Granot, *J. Power Sources* **1997**, *68*, 91.
[19] X. Liu, D. Ren, H. Hsu, Xuning Feng, Gui-Liang Xu, Minghao Zhuang, Han Gao, L. Lu, Z. Chu, J. Li, X. He, K. Amine, M. Ouyang, *Joule* **2018**, *2*, 2047.
[20] A. W. Golubkov, D. Fuchs, J. Wagner, H. Wiltsche, C. Stangl, G. Fauler, G. Voitic, A. Thaler, V. Hacker, *RSC Adv.* **2014**, *4*, 3633.
[21] F. Austin, R. Morales, C. A. Coultas-mckenney, M. J. Hargather, J. Ostanek, *J. Energy Storage* **2017**, *13*, 378.
[22] D. Ouyang, M. Chen, J. Liu, R. Wei, J. Weng, J. Wang, *RSC Adv.* **2018**, *8*, 33414.
[23] N. Sharma, V. K. Peterson, *J. Power Sources* **2013**, *244*, 695.
[24] D. Ren, X. Feng, L. Lu, M. Ouyang, S. Zheng, J. Li, X. He, *J. Power Sources* **2017**, *364*, 328.
[25] C. Lin, Y. Ren, K. Amine, Y. Qin, Z. Chen, *J. Power Sources* **2013**, *230*, 32.
[26] P. R. Shearing, M. Di Michiel, G. Hinds, J. L. Brett, P. R. Shearing, *Phys. Chem. Chem. Phys.* **2016**, *18*, 30881.

[27] J. B. Goodenough, K. S. Park, *J. Am. Chem. Soc.* **2013**, *135*, 1167.
[28] H. Wang, E. Rus, T. Sakuraba, J. Kikuchi, Y. Kiya, H. D. Abruna, *Anal. Chem.* **2014**, *86*, 6197.
[29] A. Yano, M. Shikano, A. Ueda, H. Sakaebe, Z. Ogumi, *J. Electrochem. Soc.* **2017**, *164*, A6116.
[30] N. Taguchi, T. Akita, H. Sakaebe, K. Tatsumi, Z. Ogumi, *J. Electrochem. Soc.* **2013**, *160*, A2293.
[31] N. Taguchi, H. Sakaebe, K. Tatsumi, T. Akita, *e-Journal Surf. Sci. Nanotechnol.* **2015**, *13*, 284.
[32] X. Lu, Y. Sun, Z. Jian, X. He, L. Gu, Y. S. Hu, H. Li, Z. Wang, W. Chen, X. Duan, L. Chen, J. Maier, S. Tsukimoto, Y. Ikuhara, *Nano Lett* **2012**, *12*, 6192.
[33] K.-W. Nam, S.-M. Bak, E. Hu, X. Yu, Y. Zhou, X. Wang, L. Wu, Y. Zhu, K.-Y. Chung, X.-Q. Yang, *Adv. Funct. Mater.* **2013**, *23*, 1047.
[34] A. W. Golubkov, D. Fuchs, J. Wagner, H. Wiltsche, C. Stangl, G. Fauler, G. Voitic, A. Thaler, V. Hacker, *RSC Adv.* **2014**, *4*, 3633.
[35] A. W. Golubkov, S. Scheikl, R. Planteu, G. Voitic, H. Wiltsche, C. Stangl, G. Fauler, A. Thaler, V. Hacker, *RSC Adv.* **2015**, *5*, 57171.
[36] D. P. Finegan, M. Scheel, J. B. Robinson, B. Tjaden, I. Hunt, T. J. Mason, J. Millichamp, M. Di Michiel, G. J. Offer, G. Hinds, D. J. L. Brett, P. R. Shearing, *Nat. Commun.* **2015**, *6*, 23.
[37] F. Lin, Y. Liu, X. Yu, L. Cheng, A. Singer, O. G. Shpyrko, H. L. Xin, N. Tamura, C. Tian, T. C. Weng, X. Q. Yang, Y. S. Meng, D. Nordlund, W. Yang, M. M. Doeff, *Chem. Rev.* **2017**, *117*, 13123.
[38] J. R. Dahn, E. W. Fuller, M. Obrovac, U. von Sacken, *Solid State Ionics* **1994**, *69*, 265.
[39] E. Hu, S. M. Bak, J. Liu, X. Yu, Y. Zhou, S. N. Ehrlich, X. Q. Yang, K. W. Nam, *Chem. Mater.* **2014**, *26*, 1108.
[40] N. Membreño, P. Xiao, K.-S. Park, J. B. Goodenough, G. Henkelman, K. J. Stevenson, *J. Phys. Chem. C* **2013**, *117*, 11994.
[41] T. Nishi, H. Nakai, A. Kita, *J. Electrochem. Soc.* **2013**, *160*, A1785.
[42] G. Singh, W. C. West, J. Soler, R. S. Katiyar, *J. Power Sources* **2012**, *218*, 34.
[43] K. Luo, M. R. Roberts, R. Hao, N. Guerrini, D. M. Pickup, Y. S. Liu, K. Edström, J. Guo, A. V. Chadwick, L. C. Duda, P. G. Bruce, *Nat. Chem.* **2016**, *8*, 684.
[44] D. J. Xiong, L. D. Ellis, J. Li, H. Li, T. Hynes, J. P. Allen, J. Xia, D. S. Hall, I. G. Hill, J. R. Dahn, *J. Electrochem. Soc.* **2017**, *164*, A3025.
[45] R. Jung, M. Metzger, F. Maglia, C. Stinner, H. A. Gasteiger, *J. Electrochem. Soc.* **2017**, *164*, A1361.

[46] W.-S. Yoon, K.-B. Kim, M.-G. Kim, M.-K. Lee, H.-J. Shin, J.-M. Lee, *J. Electrochem. Soc.* **2002**, *149*, A1305.
[47] D. Buchholz, J. Li, S. Passerini, G. Aquilanti, D. Wang, M. Giorgetti, *ChemElectroChem* **2015**, *2*, 85.
[48] V. A. Coleman, R. Knut, O. Karis, H. Grennberg, U. Jansson, R. Quinlan, B. C. Holloway, B. Sanyal, O. Eriksson, *J. Phys. D. Appl. Phys.* **2008**, *41*, 1.
[49] Y. W. Tsai, B. J. Hwang, G. Ceder, H. S. Sheu, D. G. Liu, J. F. Lee, *Chem. Mater.* **2005**, *17*, 3191.
[50] J. Xu, M. Sun, R. Qiao, S. E. Renfrew, L. Ma, T. Wu, S. Hwang, D. Nordlund, D. Su, K. Amine, J. Lu, B. D. McCloskey, W. Yang, W. Tong, *Nat. Commun.* **2018**, *9*, 1.
[51] S. Hwang, S. M. Kim, S. M. Bak, S. Y. Kim, B. W. Cho, K. Y. Chung, J. Y. Lee, E. A. Stach, W. Chang, *Chem. Mater.* **2015**, *27*, 3927.
[52] S. Hwang, S. M. Kim, S. M. Bak, B. W. Cho, K. Y. Chung, J. Y. Lee, W. Chang, E. A. Stach, *ACS Appl. Mater. Interfaces* **2014**, *6*, 15140.
[53] L. Wu, K. W. Nam, X. Wang, Y. Zhou, J. C. Zheng, X. Q. Yang, Y. Zhu, *Chem. Mater.* **2011**, *23*, 3953.
[54] Y. Yuan, K. Amine, J. Lu, R. Shahbazian-Yassar, *Nat. Commun.* **2017**, *8*, 1.
[55] S. M. Ghodsi, C. M. Megaridis, R. Shahbazian-yassar, *Small Methods* **2019**, *1900026*, 1.
[56] V. Yurkiv, S. Sharifi-Asl, A. Ramasubramanian, R. Shahbazian-Yassar, F. Mashayek, *Comput. Mater. Sci.* **2017**, *140*, 299.
[57] F. P. Zheng, Jiaxin, Tongchao Liu, Zongxiang Hu, Yi Wei, Xiaohe Song, Yang Ren, Weidong Wang, Mumin Rao, Yuan Lin, Zonghai Chen, Jun Lu, Chongmin Wang, Khalil Amine, *J. Am. Chem. Soc.* **2016**, *138*, 13326−13334.
[58] N. Yabuuchi, Y. Kawamoto, R. Hara, T. Ishigaki, A. Hoshikawa, M. Yonemura, T. Kamiyama, S. Komaba, *Inorg. Chem.* **2013**, *52*, 9131.
[59] H. Ben Yahia, M. Shikano, H. Kobayashi, *Chem. Mater.* **2013**, *25*, 3687.
[60] F. Lin, D. Nordlund, I. M. Markus, T.-C. Weng, H. L. Xin, M. M. Doeff, *Energy Environ. Sci.* **2014**, *7*, 3077.
[61] Chenxi Wei, Yijin Liu, Y. Zhang, *J. Mater. Chem. A* **2018**, 23055.
[62] L. Mu, R. Lin, R. Xu, L. Han, S. Xia, D. Sokaras, J. Steiner, T.-C. Weng, D. Nordlund, M. M. Doeff, Y. Liu, K. Zhao, H. L. Xin, F. Lin, *Nano Lett.* **2018**, *18*, 3241.
[63] P. Oh, B. Song, W. Li, A. Manthiram, *J. Mater. Chem. A* **2016**, *4*, 5839.
[64] P. Keil, A. Jossen, *J. Electrochem. Soc.* **2017**, *164*, A6066.
[65] F. Lin, I. M. Markus, M. M. Doeff, H. L. Xin, *Sci. Rep.* **2014**, *4*, 5694.
[66] P. Lu, P. Yan, E. Romero, E. D. Spoerke, J. G. Zhang, C. M. Wang, *Chem. Mater.* **2015**, *27*, 1375.

[67] P. J. Phillips, H. Iddir, D. P. Abraham, R. F. Klie, *Appl. Phys. Lett.* **2014**, *105*, 113905.
[68] Y. Shao-Horn, L. Croguennec, C. Delmas, E. C. Nelson, M. a O'Keefe, *Nat. Mater.* **2003**, *2*, 464.
[69] F. Xiong, H. J. Yan, Y. Chen, B. Xu, J. X. Le, C. Y. Ouyang, *Int. J. Electrochem. Sci.* **2012**, *7*, 9390.
[70] K. Mizushima, P. C. Jones, P. J. Wiseman, J. B. Goodenough, *Solid State Ionics* **1981**, *4*, 171.
[71] H. Gabrisch, R. Yazami, B. Fultz, *J. Electrochem. Soc.* **2004**, *151*, 891.
[72] H. Wang, Y. Jang, B. Huang, D. R. Sadoway, Y. Chiang, *J. Electrochem. Soc.* **1999**, *146*, 473.
[73] J. Kikkawa, S. Terada, A. Gunji, T. Nagai, K. Kurashima, K. Kimoto, *J. Phys. Chem. C* **2015**, *119*, 15823.
[74] Y. Furushima, C. Yanagisawa, T. Nakagawa, Y. Aoki, N. Muraki, *J. Power Sources* **2011**, *196*, 2260.
[75] J. Geder, H. E. Hoster, A. Jossen, J. Garche, D. Y. W. Yu, *J. Power Sources* **2014**, *257*, 286.
[76] W. Li, J. C. Currie, J. Wolstenholme, *J. Power Sources* **1997**, *68*, 565.
[77] S. Sharifi-Asl, F. A. Soto, A. Nie, Y. Yuan, H. Asayesh-Ardakani, T. Foroozan, V. Yurkiv, B. Song, F. Mashayek, R. F. Klie, K. Amine, J. Lu, P. B. Balbuena, R. Shahbazian-Yassar, *Nano Lett.* **2017**, *17*, 2165.
[78] H. Arai, Shigeto Okada, Yoji Sakurai, J. Yamaki, *Solid State Ionics* **1998**, *109*, 295.
[79] T. Ohzuku, Y. Makimura, *Chem. Lett.* **2001**, *30*, 642.
[80] B. Xu, D. Qian, Z. Wang, Y. S. Meng, *Mater. Sci. Eng. R Reports* **2012**, *73*, 51.
[81] I. Belharouak, W. Lu, J. Liu, D. Vissers, K. Amine, *J. Power Sources* **2007**, *174*, 905.
[82] I. Belharouak, W. Lu, D. Vissers, K. Amine, *Electrochem. commun.* **2006**, *8*, 329.
[83] Y. Wang, J. Jiang, J. R. Dahn, *Electrochem. commun.* **2007**, *9*, 2534.
[84] G. S. and D. A. Vinodkumar Etacheri, Rotem Marom, Ran Elazari, *Energy Environ. Sci.* **2011**, 3243.
[85] S. B. Chikkannanavar, D. M. Bernardi, L. Liu, *J. Power Sources* **2014**, *248*, 91.
[86] W. Li, X. Liu, H. Celio, P. Smith, A. Dolocan, M. Chi, A. Manthiram, *Adv. Energy Mater.* **2018**, *8*, DOI 10.1002/aenm.201703154.
[87] P. Yan, J. Zheng, J. G. Zhang, C. Wang, *Nano Lett.* **2017**, *17*, 3946.
[88] F. Lin, I. M. Markus, D. Nordlund, T.-C. Weng, M. D. Asta, H. L. Xin, M. M. Doeff, *Nat. Commun.* **2014**, *5*, 3529.

[89] J. Zhao, W. Zhang, A. Huq, S. T. Misture, B. Zhang, S. Guo, L. Wu, Y. Zhu, Z. Chen, K. Amine, F. Pan, J. Bai, F. Wang, *Adv. Energy Mater.* **2017**, *7*, 1.
[90] P. Reale, D. Privitera, S. Panero, B. Scrosati, *Solid State Ionics* **2007**, *178*, 1390.
[91] J. Wandt, A. T. S. Freiberg, A. Ogrodnik, H. A. Gasteiger, *Mater. Today* **2018**, DOI 10.1016/j.mattod.2018.03.037.
[92] C. Wei, Y. Zhang, Y. Zhang, L. Mud, J. Liu, C. Wang, Y. Yang, M. Doeff, P. Pianetta, D. Nordlund, X.-W. Du, Y. Tian, K. Zhao, h J.-S. Lee, F. Lin, Y. Liu, *J. Mater. Chem. A* **2018**, *6*, 23055.
[93] P. Yan, J. Zheng, M. Gu, J. Xiao, J. G. Zhang, C. M. Wang, *Nat. Commun.* **2017**, *8*, 1.
[94] J. M. Lim, T. Hwang, D. Kim, M. S. Park, K. Cho, M. Cho, *Sci. Rep.* **2017**, *7*, 2.
[95] P. Yan, J. Zheng, T. Chen, L. Luo, Y. Jiang, K. Wang, M. Sui, J.-G. Zhang, S. Zhang, C. Wang, *Nat. Commun.* **2018**, 1.
[96] J. Zheng, M. Gu, J. Xiao, P. Zuo, C. Wang, J. G. Zhang, *Nano Lett.* **2013**, *13*, 3824.
[97] P. Yan, J. Zheng, J. Zheng, Z. Wang, G. Teng, S. Kuppan, J. Xiao, G. Chen, F. Pan, J. G. Zhang, C. M. Wang, *Adv. Energy Mater.* **2016**, *6*, 26.
[98] Y. Wen, D. Xiao, X. Liu, L. Gu, *NPG Asia Mater.* **2017**, *9*, e360.
[99] C. Lin, A. Tang, H. Mu, W. Wang, C. Wang, *J. Chem.* **2015**, *2015*, 1.
[100] L. Wang, T. Maxisch, G. Ceder, *Chem. Mater.* **2007**, *19*, 543.
[101] N. Yabuuchi, Y. Kim, H. H. Li, Y. Shao-horn, *Chem. Mater.* **2008**, 4936.
[102] J. Reed, G. Ceder, *Chem. Rev.* **2004**, *104*, 4513.
[103] S. M. Bak, E. Hu, Y. Zhou, X. Yu, S. D. Senanayake, S. J. Cho, K. B. Kim, K. Y. Chung, X. Q. Yang, K. W. Nam, *ACS Appl. Mater. Interfaces* **2014**, *6*, 22594.
[104] W. S. Yoon, K. Y. Chung, M. Balasubramanian, J. Hanson, J. McBreen, X. Q. Yang, *J. Power Sources* **2006**, *163*, 219.
[105] Y. Yuan, A. Nie, G. M. Odegard, R. Xu, D. Zhou, S. Santhanagopalan, K. He, H. Asayesh-Ardakani, D. D. Meng, R. F. Klie, C. Johnson, J. Lu, R. Shahbazian-Yassar, *Nano Lett.* **2015**, *15*, 2998.
[106] H. Zhang, F. Omenya, P. Yan, L. Luo, M. S. Whittingham, C. Wang, G. Zhou, *ACS Energy Lett.* **2017**, *2*, 2607.
[107] S. Kuppan, A. K. Shukla, D. Membreno, D. Nordlund, G. Chen, *Adv. Electron. Mater.* **2017**, 1.
[108] D. Luo, P. shi, S. Fang, L. Yang, S. ichi Hirano, *J. Power Sources* **2017**, *364*, 121.
[109] H. Dixit, W. Zhou, J. C. Idrobo, J. Nanda, V. R. Cooper, *ACS Nano* **2014**, *8*, 12710.

[110] L. Mu, R. Lin, R. Xu, L. Han, S. Xia, D. Sokaras, J. Steiner, T.-C. Weng, D. Nordlund, M. M. Doeff, Y. Liu, K. Zhao, H. L. Xin, F. Lin, *Nano Lett.* **2018**, *18*, 3241.
[111] M. M. Thackeray, L. A. de Picciotto, A. de Kock, P. J. Johnson, V. A. Nicholas, K. T. Adendorff, *J. Power Sources* **1987**, *21*, 1.
[112] M. M. Thackeray, *J. Am. Ceram. Soc* **1999**, *82*, 3347.
[113] C. M. Julien, A. Mauger, K. Zaghib, H. Groult, *Inorganics* **2014**, *2*, 132.
[114] O. K. Park, Y. Cho, S. Lee, H.-C. Yoo, H.-K. Song, J. Cho, *Energy Environ. Sci.* **2011**, *4*, 1621.
[115] N. P. W. Pieczonka, Z. Liu, P. Lu, K. L. Olson, J. Moote, B. R. Powell, J.-H. Kim, *J. Phys. Chem. C* **2013**, *117*, 15947.
[116] D. Aurbach, B. Markovsky, Y. Talyossef, G. Salitra, H. J. Kim, S. Choi, *J. Power Sources* **2006**, *162*, 780.
[117] Y. Talyosef, B. Markovsky, G. Salitra, D. Aurbach, H. J. Kim, S. Choi, *J. Power Sources* **2005**, *146*, 664.
[118] D. Tang, Y. Sun, Z. Yang, L. Ben, L. Gu, X. Huang, *Chem. Mater.* **2014**, *26*, 3535.
[119] L. Ben, H. Yu, B. Chen, Y. Chen, Y. Gong, X. Yang, L. Gu, X. Huang, *ACS Appl. Mater. Interfaces* **2017**, *9*, 35463.
[120] E. Hu, S. M. Bak, J. Liu, X. Yu, Y. Zhou, S. N. Ehrlich, X. Q. Yang, K. W. Nam, *Chem. Mater.* **2014**, *26*, 1108.
[121] M. Brand, S. Gläser, J. Geder, S. Menacher, S. Obpacher, A. Jossen, D. Quinger, *EVS27 Int. Batter. Hybrid Fuel Cell Electr. Veh. Symp.* **2013**, 1.
[122] A. Geoffroy, HautierJain, S. P. Ong, B. Kang, C. Moore, R. Doe, G. Ceder, *Chem. Mater.* **2011**, 3495.
[123] G. Chen, T. J. Richardson, *J. Power Sources* **2010**, *195*, 1221.
[124] A. S. Andersson, J. O. Thomas, B. Kalska, L. Häggström, *Electrochem. Solid-State Lett* **2000**, *3*, 66.
[125] R. Malik, F. Zhou, G. Ceder, *Nat. Mater.* **2011**, *10*, 587.
[126] Z. X. Nie, C. Y. Ouyang, J. Z. Chen, Z. Y. Zhong, Y. L. Du, D. S. Liu, S. Q. Shi, M. S. Lei, *Solid State Commun.* **2010**, *150*, 40.
[127] S. Theil, M. Fleischhammer, P. Axmann, M. Wohlfahrt-mehrens, *J. Power Sources* **2013**, *222*, 72.
[128] D. A. Surendra K. Martha, Ortal Haik, Ella Zinigrad, Ivan Exnar, Thierry Drezen, James H. Miners, *J. Electrochem. Soc.* **2011**, *158*, 1115.
[129] S. P. Ong, A. Jain, G. Hautier, B. Kang, G. Ceder, *Electrochem. commun.* **2010**, *12*, 427.
[130] Z. Lu, L. Y. Beaulieu, R. A. Donaberger, C. L. Thomas, J. R. Dahn, *J. Electrochem. Soc.* **2002**, *149*, A778.
[131] M. M. Thackeray, C. S. Johnson, J. T. Vaughey, N. LiCurrent address:

eVionyx Inc., Ha, S. A. Hackney, *J. Mater. Chem.* **2005**, *15*, 2257.
[132] B. Qiu, M. Zhang, Y. Xia, Z. Liu, Y. S. Meng, *Chem. Mater.* **2017**, *29*, 2.
[133] J. Zheng, S. Myeong, W. Cho, P. Yan, J. Xiao, C. Wang, J. Cho, J. Zhang, *Adv. Energy Mater.* **2017**, 1.
[134] M. Sathiya, G. Rousse, K. Ramesha, C. P. Laisa, H. Vezin, M. T. Sougrati, M.-L. Doublet, D. Foix, D. Gonbeau, W. Walker, a S. Prakash, M. Ben Hassine, L. Dupont, J.-M. Tarascon, *Nat. Mater.* **2013**, *12*, 827.
[135] J. Yan, X. Liu, B. Li, *RSC Adv.* **2014**, *4*, 63268.
[136] H. Yu, H. Zhou, *J. Phys. Chem. Lett.* **2013**, *4*, 1268.
[137] A. K. Shukla, Q. M. Ramasse, C. Ophus, H. Duncan, F. Hage, G. Chen, *Nat. Commun.* **2015**, *6*, 1.
[138] J. R. Croy, M. Balasubramanian, K. G. Gallagher, A. K. Burrell, *Acc. Chem. Res.* **2015**, *48*, 2813.
[139] M. Sathiya, A. M. Abakumov, D. Foix, G. Rousse, K. Ramesha, M. Saubanère, M. L. Doublet, H. Vezin, C. P. Laisa, a S. Prakash, D. Gonbeau, G. VanTendeloo, J.-M. Tarascon, *Nat. Mater.* **2015**, *14*, 230.
[140] A. Boulineau, L. Croguennec, C. Delmas, F. Weill, *Chem. Mater.* **2009**, *21*, 4216.
[141] G. Yang, H. Ji, P. Gao, A. Hong, H. Ding, S. Roy, J. Pinto, X. Jiang, *J. Electrochem. Soc.* **2011**, *158*, A1071.
[142] A. R. Armstrong, M. Holzapfel, P. Novák, C. S. Johnson, S. H. Kang, M. M. Thackeray, P. G. Bruce, *J. Am. Chem. Soc.* **2006**, *128*, 8694.
[143] A. R. Armstrong, M. Holzapfel, P. Novak, C. S. Johnson, S.-H. Kang, M. M. Thackeray, P. G. Bruce, *J. Am. Chem. Soc.* **2006**, *128*, 8694.
[144] J. Hong, H. D. Lim, M. Lee, S. W. Kim, H. Kim, S. T. Oh, G. C. Chung, K. Kang, *Chem. Mater.* **2012**, *24*, 2692.
[145] E. Hu, S. M. Bak, Y. Liu, J. Liu, X. Yu, Y. N. Zhou, J. Zhou, P. Khalifah, K. Ariyoshi, K. W. Nam, X. Q. Yang, *Adv. Energy Mater.* **2016**, *6*, 1.
[146] A. Singer, M. Zhang, S. Hy, D. Cela, C. Fang, T. A. Wynn, B. Qiu, Y. Xia, Z. Liu, A. Ulvestad, N. Hua, J. Wingert, H. Liu, M. Sprung, A. V. Zozulya, E. Maxey, R. Harder, Y. S. Meng, O. G. Shpyrko, *Nat. Energy* **2018**, *3*, 1.
[147] D.-H. Seo, J. Lee, A. Urban, R. Malik, S. Kang, G. Ceder, *Nat. Chem.* **2016**, *8*, 692.
[148] H. Chen, M. S. Islam, *Chem. Mater.* **2016**, *28*, DOI 10.1021/acs.chemmater.6b02870.
[149] H. Chen, M. S. Islam, *Chem. Mater.* **2016**, *28*, 6656.
[150] S. Bhowmick, A. Sadrzadeh, B. I. Yakobson, E. S. Penev, B. I. Yakobson, J. Gao, J. Zhao, V. V Struzhkin, H. Mao, R. J. Hemley, C. W. Glass, L. Li, A. R. Oganov, P. B. Allen, S. Curtarolo, X. Wei, J. W. Kysar, J. Hone, *Science (80-.).* **2015**, *350*, 1516.

[151] A. Marusczyk, J.-M. Albina, T. Hammerschmidt, R. Drautz, T. Eckl, G. Henkelman, *J. Mater. Chem. A* **2017**, *5*, 15183.
[152] P. E. Pearce, A. J. Perez, G. Rousse, M. Saubanère, D. Batuk, D. Foix, E. McCalla, A. M. Abakumov, G. Van Tendeloo, M.-L. Doublet, J.-M. Tarascon, *Nat. Mater.* **2017**, *16*, 580.
[153] H. Liu, K. J. Harris, M. Jiang, Y. Wu, G. R. Goward, G. A. Botton, *ACS Nano* **2018**, *12*, 2708.
[154] M. Gu, I. Belharouak, J. Zheng, H. Wu, J. Xiao, A. Genc, K. Amine, S. Thevuthasan, D. R. Baer, J. G. Zhang, N. D. Browning, J. Liu, C. Wang, *ACS Nano* **2013**, *7*, 760.
[155] J. Jiang, J. R. Dahn, *Electrochim. Acta* **2005**, *50*, 4778.
[156] J. Cho, T. Kim, C. Kim, J. Lee, Y. Kim, B. Park, *J. Power Sources* **2005**, *146*, 58.
[157] H. Konishi, T. Hirano, D. Takamatsu, A. Gunji, X. Feng, S. Furutsuki, *Electrochim. Acta* **2015**, *186*, 591.
[158] H. Konishi, T. Hirano, D. Takamatsu, A. Gunji, X. Feng, S. Furutsuki, *Electrochim. Acta* **2015**, *169*, 310.
[159] C. K. Lin, Y. Piao, Y. Kan, J. Bareño, I. Bloom, Y. Ren, K. Amine, Z. Chen, *ACS Appl. Mater. Interfaces* **2014**, *6*, 12692.
[160] N. Li, Y. S. He, X. Wang, W. Zhang, Z. F. Ma, D. Zhang, *Electrochim. Acta* **2017**, *231*, 363.
[161] D. Wang, M. Liu, X. Wang, R. Yu, G. Wang, Q. Ren, X. Yang, *RSC Adv.* **2016**, *6*, 57310.
[162] S. Yu, C. Peng, Z. Li, L. Zhang, Q. Xiao, G. Lei, Y. Ding, *Arab. J. Sci. Eng.* **2017**, *42*, 4291.
[163] Z. Zheng, X. D. Guo, Y. J. Zhong, W. B. Hua, C. H. Shen, S. L. Chou, X. S. Yang, *Electrochim. Acta* **2016**, *188*, 336.
[164] D. Vu, J. Lee, *J. Solid State Electrochem.* **2017**, *2*, 1165.
[165] Y. Liu, D. Ning, L. Zheng, Q. Zhang, L. Gu, R. Gao, J. Zhang, A. Franz, G. Schumacher, X. Liu, *J. Power Sources* **2018**, *375*, 1.
[166] Y. Sun, L. Zhang, Y. Zhou, Y. Shen, C. Hai, X. Li, J. Zeng, X. Ren, L. Ma, X. Zhang, S. Dong, G. Qi, *J. Electrochem. Soc.* **2018**, *165*, A333.
[167] S. H. Min, M. R. Jo, S. Y. Choi, Y. Il Kim, Y. M. Kang, *Adv. Energy Mater.* **2016**, *6*, 1501717.
[168] H. Liu, Q. Cao, L. J. Fu, C. Li, Y. P. Wu, H. Q. Wu, *Electrochem. commun.* **2006**, *8*, 1553.
[169] C. P. Laisa, R. N. Ramesha, K. Ramesha, *Electrochim. Acta* **2017**, *256*, 10.
[170] A. Liu, J. Li, R. Shunmugasundaram, J. R. Dahn, *J. Electrochem. Soc.* **2017**, *164*, A1655.
[171] C. Bellitto, E. M. Bauer, G. Righini, M. A. Green, W. R. Branford, A.

Antonini, M. Pasquali, *J. Phys. Chem. Solids* **2004**, *65*, 29.
[172] P. K. Nayak, J. Grinblat, E. Levi, M. Levi, B. Markovsky, D. Aurbach, *Phys. Chem. Chem. Phys.* **2017**, *19*, 6142.
[173] Webin Luo, X. Li, J. R. Dahn, *Chem. Mater.* **2010**, *22*, 5065.
[174] A. Iqbal, Y. Iqbal, L. Chang, S. Ahmed, Z. Tang, Y. Gao, *J. Nanoparticle Res.* **2012**, *14*, 1206.
[175] J. R. D. Wenbin Luo, Fu Zhou, Xuemei Zhao, Zhonghua Lu, Xinhai Li, *Chem. Mater.* **2010**, *22*, 1164.
[176] Y. Luo, T. Lu, Y. Zhang, L. Yan, S. S. Mao, J. Xie, *J. Alloys Compd.* **2017**, *703*, 289.
[177] X. Hu, H. Guo, W. Peng, Z. Wang, X. Li, Q. Hu, *J. Electroanal. Chem.* **2018**, *822*, 57.
[178] M. Li, Y. Zhou, X. Wu, L. Duan, C. Zhang, F. Zhang, D. He, *Electrochim. Acta* **2018**, *275*, 18.
[179] Milad Ghorbanzadeh, E. Allahyari, Reza Riahifar, S. M. M. Hadavi, *J. Solid State Electrochem.* **2018**, *22*, 1155.
[180] H. Guo, Y. Xia, H. Zhao, C. Yin, K. Jia, F. Zhao, Z. Liu, *Ceram. Int.* **2017**, *43*, 13845.
[181] R. N. Ramesha, C. P. Laisa, K. Ramesha, *Electrochim. Acta* **2017**, *249*, 377.
[182] R. Yu, G. Wang, M. Liu, X. Zhang, X. Wang, H. Shu, X. Yang, W. Huang, *J. Power Sources* **2016**, *335*, 65.
[183] G. Xu, Q. Xue, J. Li, Z. Li, X. Li, T. Yu, J. Li, X. Wang, F. Kang, *Solid State Ionics* **2016**, *293*, 7.
[184] F. Zhou, X. Zhao, Z. Lu, J. Jiang, J. R. Dahn, *J. Electrochem. Soc.* **2008**, *11*, 155.
[185] L. Croguennec, J. Bains, J. Bre, C. Tessier, S. Levasseur, C. Delmas, *J. Electrochem. Soc.* **2011**, *158*, 664.
[186] H. Lin, C. Liang, M. Li, C. Dai, Y. Xiong, *Energy Technol.* **2017**, *5*, 1472.
[187] C. P. Laisa, A. K. Nanda Kumar, S. Selva Chandrasekaran, P. Murugan, N. Lakshminarasimhan, R. Govindaraj, K. Ramesha, *J. Power Sources* **2016**, *324*, 462.
[188] L. Pan, Y. Xia, B. Qiu, H. Zhao, H. Guo, K. Jia, Q. Gu, Z. Liu, *J. Power Sources* **2016**, *327*, 273.
[189] R. Yu, Z. Zhang, S. Jamil, J. Chen, X. Zhang, X. Wang, Z. Yang, H. Shu, X. Yang, *ACS Appl. Mater. Interfaces* **2018**, *10*, 16561.
[190] P. K. Nayak, J. Grinblat, M. Levi, E. Levi, S. Kim, J. W. Choi, D. Aurbach, *Adv. Energy Mater.* **2016**, *6*, 1.
[191] W. Yan, Y. Xie, J. Jiang, D. Sun, X. Ma, Z. Lan, Y. Jin, *ACS Sustain. Chem. Eng.* **2018**, *6*, 4625.
[192] B. Yue, X. Wang, J. Wang, J. Yao, X. Zhao, H. Zhang, W. Yu, G. Liu, X.

Dong, *RSC Adv.* **2018**, *8*, 4112.
[193] L. Zhao, Q. Wu, J. Wu, *J. Solid State Electrochem.* **2018**, *22*, 2141.
[194] H. Wang, T. A. Tan, P. Yang, M. O. Lai, L. Lu, *J. Phys. Chem. C* **2011**, *115*, 6102.
[195] S. Myung, S. Komaba, K. Hosoya, N. Hirosaki, Y. Miura, N. Kumagai, *J. Solid State Electrochem.* **2005**, 2427.
[196] K. C. Kam, A. Mehta, J. T. Heron, M. M. Doeff, S. Radiation, S. National, M. Park, *J. Electrochem. Soc.* **2012**, *159*, 1383.
[197] L. Zhou, J. Liu, L. Huang, N. Jiang, Q. Zheng, D. Lin, *J. Solid State Electrochem.* **2017**, *21*, 3467.
[198] C. Lu, S. Yang, H. Wu, Y. Zhang, X. Yang, T. Liang, *Electrochim. Acta* **2016**, *209*, 448.
[199] H. Wang, T. A. Tan, P. Yang, M. O. Lai, L. Lu, *J. Phys. Chem. C* **2011**, *115*, 6102.
[200] Y. Zhao, M. Xia, X. Hu, Z. Zhao, Y. Wang, Z. Lv, *Electrochim. Acta* **2015**, *174*, 1167.
[201] E. Han, X. Du, P. Yang, Y. Han, *Ionics (Kiel).* **2017**, 393.
[202] K. Hoang, *Phys. Rev. Mater.* **2017**, *1*, 075404.
[203] Q. Li, G. Li, C. Fu, D. Luo, J. Fan, L. Li, *ACS Appl. Mater. Interfaces* **2014**, *6*, 10330.
[204] W. Cho, S. Myeong, N. Kim, S. Lee, Y. Kim, M. Kim, S. J. Kang, N. Park, P. Oh, J. Cho, *Adv. Mater.* **2017**, *29*, 1605578.
[205] R. Yu, X. Wang, Y. Fu, L. Wang, S. Cai, M. Liu, B. Lu, G. Wang, D. Wang, Q. Ren, X. Yang, *J. Mater. Chem. A* **2016**, *4*, 4941.
[206] F. Zhou, X. Zhao, Z. Lu, J. Jiang, J. R. Dahn, *Electrochem. Commun. J.* **2008**, *10*, 1168.
[207] W. Luo, J. R. Dahn, *J. Electrochem. Soc.* **2011**, *158*, 428.
[208] A. Kapylou, J. H. Song, A. Missiul, D. J. Ham, D. H. Kim, S. Moon, J. H. Park, *ChemPhysChem* **2018**, *19*, 116.
[209] S. Liu, Z. Wang, Y. Huang, Z. Ni, J. Bai, S. Kang, Y. Wang, X. Li, *J. Alloys Compd.* **2018**, *731*, 636.
[210] F. Kong, C. Liang, R. C. Longo, D. H. Yeon, Y. Zheng, J. H. Park, S. G. Doo, K. Cho, *Chem. Mater.* **2016**, *28*, 6942.
[211] L. Ming, B. Zhang, Y. Cao, J.-F. Zhang, C.-H. Wang, X.-W. Wang, H. Li, *Front. Chem.* **2018**, *6*, 1.
[212] B. Guo, J. Zhao, X. Fan, W. Zhang, S. Li, Z. Yang, Z. Chen, W. Zhang, *Electrochim. Acta* **2017**, *236*, 171.
[213] Y.-J. Kang, J.-H. Kim, Y.-K. Sun, *J. Power Sources* **2005**, *146*, 237.
[214] Y. K. Sun, Z. Chen, H. J. Noh, D. J. Lee, H. G. Jung, Y. Ren, S. Wang, C. S. Yoon, S. T. Myung, K. Amine, *Nat. Mater.* **2012**, *11*, 942.

[215] J. Li, R. Doig, J. Camardese, K. Plucknett, J. R. Dahn, *Chem. Mater.* **2015**, *27*, 7765.
[216] S.-T. Myung, H.-J. Noh, S.-J. Yoon, E.-J. Lee, Y.-K. Sun, *J. Phys. Chem. Lett.* **2014**, *5*, 671.
[217] C. S. Yoon, S. J. Kim, U.-H. Kim, K. Park, H. Ryu, H. Kim, Y. Sun, *Adv. Funct. Mater.* **2018**, *28*, 1802090.
[218] K.-J. Park, M.-J. Choi, F. Maglia, S.-J. Kim, K.-H. Kim, C. S. Yoon, Y.-K. Sun, *Adv. Energy Mater.* **2018**, *8*, 1703612.
[219] B. B. Lim, S. J. Yoon, K. J. Park, C. S. Yoon, S. J. Kim, J. J. Lee, Y. K. Sun, *Adv. Funct. Mater.* **2015**, *25*, 4673.
[220] Y. K. Sun, D. H. Kim, C. S. Yoon, S. T. Myung, J. Prakash, K. Amine, *Adv. Funct. Mater.* **2010**, *20*, 485.
[221] J. W. Ju, E. J. Lee, C. S. Yoon, S. T. Myung, Y. K. Sun, *J. Phys. Chem. C* **2014**, *118*, 175.
[222] Y. K. Sun, B. R. Lee, H. J. Noh, H. Wu, S. T. Myung, K. Amine, *J. Mater. Chem.* **2011**, *21*, 10108.
[223] P. Y. Hou, L. Q. Zhang, X. P. Gao, *J. Mater. Chem. A* **2014**, *2*, 17130.
[224] R. C. Longo, C. Liang, F. Kong, K. Cho, *ACS Appl. Mater. Interfaces* **2018**, *10*, 19226.
[225] S. Chong, Y. Wu, Y. Chen, C. Shu, Y. Liu, *J. Power Sources* **2017**, *356*, 153.
[226] J. Ahn, J. H. Kim, B. W. Cho, K. Y. Chung, S. Kim, J. W. Choi, S. H. Oh, *Nano Lett.* **2017**, *17*, 7869.
[227] Y. Sun, S. Myung, M. Kim, J. Prakash, K. Amine, *J. Am. Chem. Soc.* **2005**, *8*, 13411.
[228] N. H. Vu, P. Arunkumar, J. C. Im, W. Bin Im, *J. Alloys Compd.* **2017**, *704*, 459.
[229] S. Kalluri, M. Yoon, M. Jo, H. K. Liu, S. X. Dou, J. Cho, Z. Guo, *Adv. Mater.* **2017**, *29*, 1605807.
[230] L. Hu, P. Brüner, T. Grehl, H. H. Brongersma, J. Cabana, *Chem. Mater.* **2017**, *29*, 5896.
[231] X. D. Zhang, J. L. Shi, J. Y. Liang, Y. X. Yin, J. N. Zhang, X. Q. Yu, Y. G. Guo, *Adv. Mater.* **2018**, *30*, 1.
[232] Y. Cho, S. Lee, Y. Lee, T. Hong, J. Cho, *Adv. Energy Mater.* **2011**, *1*, 821.
[233] B. Qiu, M. Zhang, L. Wu, J. Wang, Y. Xia, D. Qian, H. Liu, S. Hy, Y. Chen, K. An, Y. Zhu, Z. Liu, Y. S. Meng, *Nat. Commun.* **2016**, *7*, 12108.
[234] J. Cho, Y.-W. Kim, B. Kim, J.-G. Lee, B. Park, *Angew. Chemie Int. Ed.* **2003**, *42*, 1618.
[235] J. Cho, *Electrochim. Acta* **2003**, *48*, 2807.
[236] J. Cho, *Electrochem. commun.* **2003**, *5*, 146.
[237] A. T. Appapillai, A. N. Mansour, J. Cho, Y. Shao-Horn, *Chem. Mater.* **2007**,

19, 5748.
[238] Y. Lu, A. N. Mansour, N. Yabuuchi, Y. Shao-horn, *Chem. Mater.* **2009**, *21*, 4408.
[239] B. Xiao, B. Wang, J. Liu, K. Kaliyappan, Q. Sun, Y. Liu, G. Dadheech, M. P. Balogh, L. Yang, T. K. Sham, R. Li, M. Cai, X. Sun, *Nano Energy* **2017**, *34*, 120.
[240] Z. Wang, H.-Q. Lu, Y.-P. Yin, X.-Y. Sun, X.-T. Bai, X.-L. Shen, W.-D. Zhuang, S.-G. Lu, *Rare Met.* **2017**, *36*, 899.
[241] Y. Lee, J. Lee, K. Y. Lee, J. Mun, J. K. Lee, W. Choi, *J. Power Sources* **2016**, *315*, 284.
[242] Z. Wang, S. Luo, J. Ren, D. Wang, X. Qi, *Appl. Surf. Sci.* **2016**, *370*, 437.
[243] H. Liu, C. Chen, C. Du, X. He, G. Yin, B. Song, P. Zuo, X. Cheng, Y. Ma, Y. Gao, *J. Mater. Chem. A* **2015**, *3*, 2634.
[244] F. Wu, X. Zhang, T. Zhao, L. Li, M. Xie, R. Chen, *J. Mater. Chem. A* **2015**, *3*, 9528.
[245] Q. Q. Qiao, H. Z. Zhang, G. R. Li, S. H. Ye, C. W. Wang, X. P. Gao, *J. Mater. Chem. A* **2013**, *1*, 5262.
[246] F. Ding, J. Li, F. Deng, G. Xu, Y. Liu, K. Yang, F. Kang, *ACS Appl. Mater. Interfaces* **2017**, *9*, 27936.
[247] W. Liu, P. Oh, X. Liu, S. Myeong, W. Cho, J. Cho, *Adv. Energy Mater.* **2015**, *5*, 1.
[248] H. Kweon, J. Park, J. Seo, G. Kim, B. Jung, H. S. Lim, *J. Power Sources* **2004**, *126*, 156.
[249] I. D. Scott, Y. S. Jung, A. S. Cavanagh, Y. Yan, A. C. Dillon, S. M. George, S. H. Lee, *Nano Lett.* **2011**, *11*, 414.
[250] K. Du, H. Xie, G. Hu, Z. Peng, Y. Cao, F. Yu, *ACS Appl. Mater. Interfaces* **2016**, *8*, 17713.
[251] J. Kang, B. Han, *ACS Appl. Mater. Interfaces* **2015**, *7*, 11599.
[252] S. C. Jung, Y. K. Han, *J. Phys. Chem. Lett.* **2013**, *4*, 2681.
[253] S. C. Jung, H. J. Kim, J. W. Choi, Y. K. Han, *Nano Lett.* **2014**, *14*, 6559.
[254] Y. Su, S. Cui, Z. Zhuo, W. Yang, X. Wang, F. Pan, *ACS Appl. Mater. Interfaces* **2015**, *7*, 25105.
[255] P. Yan, J. Zheng, X. Zhang, R. Xu, K. Amine, J. Xiao, J. G. Zhang, C. M. Wang, *Chem. Mater.* **2016**, *28*, 857.
[256] X. Fang, F. Lin, D. Nordlund, M. Mecklenburg, M. Ge, J. Rong, A. Zhang, C. Shen, Y. Liu, Y. Cao, M. M. Doeff, C. Zhou, *Adv. Funct. Mater.* **2017**, *27*, 1.
[257] T. Teranishi, Y. Yoshikawa, M. Yoneda, A. Kishimoto, J. Halpin, S. O'Brien, M. Modreanu, I. M. Povey, *ACS Appl. Energy Mater.* **2018**, acsaem.8b00496.

[258] A. Zhou, Y. Lu, Q. Wang, J. Xu, W. Wang, X. Dai, J. Li, *J. Power Sources* **2017**, *346*, 24.
[259] C. Zhang, J. Su, T. Wang, K. Yuan, C. Chen, S. Liu, T. Huang, J. H. Wu, H. Lu, A. Yu, *ACS Sustain. Chem. Eng.* **2018**, *6*, 7890.
[260] H.-M. Cho, M. V. Chen, A. C. MacRae, Y. S. Meng, *ACS Appl. Mater. Interfaces* **2015**, *7*, 16231.
[261] B. Qiu, J. Wang, Y. Xia, Z. Wei, S. Han, Z. Liu, *ACS Appl. Mater. Interfaces* **2014**, *6*, 9185.
[262] J. Zhao, Y. Wang, *J. Phys. Chem. C* **2012**, *116*, 11867.
[263] X. Dai, L. Wang, J. Xu, Y. Wang, A. Zhou, J. Li, *ACS Appl. Mater. Interfaces* **2014**, *6*, 15853.
[264] Y.-K. Sun, K.-J. Hong, J. Prakash, *J. Electrochem. Soc.* **2003**, *150*, A970.
[265] M. R. Laskar, D. H. K. Jackson, S. Xu, R. J. Hamers, D. Morgan, T. F. Kuech, *ACS Appl. Mater. Interfaces* **2017**, *9*, 11231.
[266] Y. Jin, S. Lee, H. Lim, B. Moon, K. Han, J. Kim, J. Song, J. Yu, W. Cho, M. Park, *Electrochim. Acta* **2018**, *282*, 311.
[267] Y. C. Li, W. M. Zhao, W. Xiang, Z. G. Wu, Z. G. Yang, C. L. Xu, Y. Di Xu, E. H. Wang, C. J. Wu, X. D. Guo, *J. Alloys Compd.* **2018**, *766*, 546.
[268] S. Zhang, H. Gu, T. Tang, W. Du, M. Gao, Y. Liu, D. Jian, H. Pan, *ACS Appl. Mater. Interfaces* **2017**, *9*, 33863.
[269] A. Zhou, W. Wang, Q. Liu, Y. Wang, X. Yao, F. Qing, E. Li, T. Yang, L. Zhang, J. Li, *J. Power Sources* **2017**, *362*, 131.
[270] B. Han, T. Paulauskas, B. Key, C. Peebles, J. S. Park, R. F. Klie, J. T. Vaughey, F. Dogan, *ACS Appl. Mater. Interfaces* **2017**, *9*, 14769.
[271] H. Meng, L. Li, J. Liu, X. Han, W. Zhang, X. Liu, Q. Xu, *J. Alloys Compd.* **2017**, *690*, 256.
[272] Y. Deng, J. Mou, H. Wu, N. Jiang, Q. Zheng, K. H. Lam, C. Xu, D. Lin, *Electrochim. Acta* **2017**, *235*, 19.
[273] A. Zhou, X. Dai, Y. Lu, Q. Wang, M. Fu, J. Li, *ACS Appl. Mater. Interfaces* **2016**, *8*, 34123.
[274] C. Chen, T. Geng, C. Du, P. Zuo, X. Cheng, Y. Ma, G. Yin, *J. Power Sources* **2016**, *331*, 91.
[275] Q. Fu, F. Du, X. Bian, Y. Wang, X. Yan, Y. Zhang, K. Zhu, G. Chen, C. Wang, Y. Wei, *J. Mater. Chem. A* **2014**, *2*, 7555.
[276] H.-M. Cheng, F.-M. Wang, J. P. Chu, R. Santhanam, J. Rick, S.-C. Lo, *J. Phys. Chem. C* **2012**, *116*, 7629.
[277] J.-H. Shim, S. Lee, S. S. Park, *Chem. Mater.* **2014**, *26*, 2537.
[278] F. Wu, J. Liu, L. Li, X. Zhang, R. Luo, Y. Ye, R. Chen, *ACS Appl. Mater. Interfaces* **2016**, *8*, 23095.
[279] Z. Liu, P. Hu, J. Ma, B. Qin, Z. Zhang, C. Mou, Y. Yao, G. Cui, *Electrochim.*

Acta **2017**, *236*, 221.
[280] P. Xue, D. Gao, S. Chen, S. Zhao, B. Wang, L. Li, *RSC Adv.* **2014**, *4*, 52624.
[281] J. S. Park, A. U. Mane, J. W. Elam, J. R. Croy, *Chem. Mater.* **2015**, *27*, 1917.
[282] J. Xie, A. D. Sendek, E. D. Cubuk, X. Zhang, Z. Lu, Y. Gong, T. Wu, F. Shi, W. Liu, E. J. Reed, Y. Cui, *ACS Nano* **2017**, *11*, 7019.
[283] Y. K. Sun, J. M. Han, S. T. Myung, S. W. Lee, K. Amine, *Electrochem. commun.* **2006**, *8*, 821.
[284] Y. Zhou, Y. Lee, H. Sun, J. M. Wallas, S. M. George, M. Xie, *ACS Appl. Mater. Interfaces* **2017**, *9*, 9614.
[285] E. Hu, X. Yu, R. Lin, X. Bi, J. Lu, S. Bak, K. W. Nam, H. L. Xin, C. Jaye, D. A. Fischer, K. Amine, X. Q. Yang, *Nat. Energy* **2018**, *3*, 690.
[286] M. Chen, K. Kou, M. Tu, J. Hu, X. Du, B. Yang, *Solid State Ionics* **2017**, *310*, 95.
[287] C.-H. Lai, D. S. Ashby, T. C. Lin, J. Lau, A. Dawson, S. H. Tolbert, B. S. Dunn, *Chem. Mater.* **2018**, *30*, 2589.
[288] Y. S. Lee, W. K. Shin, A. G. Kannan, S. M. Koo, D. W. Kim, *ACS Appl. Mater. Interfaces* **2015**, *7*, 13944.
[289] S. Chen, T. He, Y. Su, Y. Lu, L. Bao, L. Chen, Q. Zhang, J. Wang, R. Chen, F. Wu, *ACS Appl. Mater. Interfaces* **2017**, *9*, 29732.
[290] J. Ha, S.-K. Park, S.-H. Yu, A. Jin, B. Jang, S. Bong, I. Kim, Y.-E. Sung, Y. Piao, *Nanoscale* **2013**, *5*, 8647.
[291] I. T. Kim, J. C. Knight, H. Celio, A. Manthiram, *J. Mater. Chem. A* **2014**, *2*, 8696.
[292] H. Xu, J. Chang, J. Sun, L. Gao, *Mater. Lett.* **2012**, *83*, 27.
[293] J.-H. Shim, Y.-M. Kim, M. Park, J. Kim, S. Lee, *ACS Appl. Mater. Interfaces* **2017**, *9*, 18720.
[294] K. S. Chen, R. Xu, N. S. Luu, E. B. Secor, K. Hamamoto, Q. Li, S. Kim, V. K. Sangwan, I. Balla, L. M. Guiney, J. W. T. Seo, X. Yu, W. Liu, J. Wu, C. Wolverton, V. P. Dravid, S. A. Barnett, J. Lu, K. Amine, M. C. Hersam, *Nano Lett.* **2017**, *17*, 2539.
[295] P. Oh, M. Ko, S. Myeong, Y. Kim, J. Cho, *Adv. Energy Mater.* **2014**, *4*, 1400631.